

This is a repository copy of *Theoretical rheo-physics of silk: Intermolecular associations reduce the critical specific work for flow-induced crystallization*.

White Rose Research Online URL for this paper:

<https://eprints.whiterose.ac.uk/185057/>

Version: Accepted Version

---

**Article:**

McLeish, Thomas Charles [orcid.org/0000-0002-2025-0299](https://orcid.org/0000-0002-2025-0299) and Schaefer, Charley (2022) Theoretical rheo-physics of silk: Intermolecular associations reduce the critical specific work for flow-induced crystallization. *Journal of Rheology*. pp. 515-534. ISSN 1520-8516

<https://doi.org/10.1122/8.0000411>

---

**Reuse**

This article is distributed under the terms of the Creative Commons Attribution (CC BY) licence. This licence allows you to distribute, remix, tweak, and build upon the work, even commercially, as long as you credit the authors for the original work. More information and the full terms of the licence here:

<https://creativecommons.org/licenses/>

**Takedown**

If you consider content in White Rose Research Online to be in breach of UK law, please notify us by emailing [eprints@whiterose.ac.uk](mailto:eprints@whiterose.ac.uk) including the URL of the record and the reason for the withdrawal request.

This is the author's peer reviewed, accepted manuscript. However, the online version of record will be different from this version once it has been copyedited and typeset.

PLEASE CITE THIS ARTICLE AS DOI: 10.1122/8.0000411

1 **Theoretical rheo-physics of silk: Intermolecular associations reduce the critical**  
2 **specific work for flow-induced crystallisation**

3 Charley Schaefer<sup>1, a)</sup> and Tom C. B. McLeish<sup>1</sup>

4 *Department of Physics, University of York, Heslington, York, YO10 5DD,*  
5 *UK*

6 (Dated: 18 February 2022)

Silk is a semi-dilute solution of randomly coiled associating polypeptide chains that crystallise following the stretch-induced disruption, in the strong extensional flow of extrusion, of the solvation shell around their amino acids. We propose that natural silk spinning exploits both the exponentially-broad stretch-distribution generated by associating polymers in extensional flow and the criterion of a critical concentration of sufficiently-stretched chains to nucleate flow-induced crystallisation. To investigate the specific-energy input needed to reach this criterion in start-up flow, we have coupled a model for the Brownian dynamics of a bead-spring-type chain, whose beads represent coarse-grained Gaussian chain segments, to the stochastic, strain-dependent binding and unbinding of their associations. We have interpreted the simulations with the aid of analytic calculations on simpler, tractable models with the same essential physical features. Our simulations indicate that the associations hamper chain alignment in the initial slow flow, but, on the other hand, facilitate chain stretching at low specific work at later, high rates. We identify a minimum in the critical specific work at a strain rate just above the stretch transition (i.e, where the mean stretch diverges), which we explain in terms of analytical solutions of a two-state master equation. We further discuss how the silkworm appears to exploit the chemical tunability of the associations to optimise chain alignment and stretching in different locations along the spinning duct: this delicate mechanism also highlights the potential biomimetic industrial benefits of chemically tunable processing of synthetic association polymers.

<sup>a)</sup>Electronic mail: charley.schaefer@york.ac.uk

This is the author's peer reviewed, accepted manuscript. However, the online version of record will be different from this version once it has been copyedited and typeset.

PLEASE CITE THIS ARTICLE AS DOI: 10.1122/1.5000041

## 7 I. INTRODUCTION

8 The manufacturing of both natural and artificial polymer-based fibres relies on flow-  
9 induced crystallisation in non-linear rheological conditions<sup>1-6</sup>. The energy input required by  
10 this process may be significantly reduced in natural silk-spinning, though the mechanism by  
11 which this efficiency is achieved has been far from clear<sup>7</sup>. There is evidence, however, that  
12 locally-tailored macromolecular interactions are involved<sup>8-11</sup>: The silk protein, of which  
13 the conformation in solution closely resembles a random coil<sup>12</sup>, self-assembles in flow in  
14 aqueous conditions under energy requirements orders of magnitude lower than its synthetic  
15 counterparts<sup>7</sup>. It has been hypothesised that flow-induced stretching of the chain disrupts a  
16 solvation layer and in turn enables crystallisation to commence<sup>7,13,14</sup>. This mechanism was  
17 supported by molecular dynamics simulations<sup>15-18</sup>, and was employed to induce crystallisa-  
18 tion of synthetic poly-ethylene oxide by flow at similarly low energetic requirements as silk,  
19 however, at much higher molecular weight and/or strain rates<sup>13</sup>. The low-energy mecha-  
20 nism for natural silk-spinning therefore remains to be identified. Clues may be present in  
21 the subtle electrostatically-modified rheo-physics of associating polymers<sup>19-28</sup>.

22 We previously found, in collaboration with Laity and Holland, that the silk protein ex-  
23 hibits calcium bridges that act as intermolecular reversible cross-links<sup>8,9</sup>. Such associations,  
24 sometimes referred to as 'stickers' that can be in a bound/closed or unbound/open state<sup>19</sup>,  
25 shift the alignment-to-stretch transition to smaller strain rates by replacing the usual Rouse  
26 relaxation dynamics for 'sticky Rouse' relaxation<sup>19-28</sup>. Inspired by these observations, we  
27 envision a mechanism of flow-induced crystallisation where the reversible network is ini-  
28 tially equilibrated (in stark contrast to the typical mechanism for the sol-gel transition of  
29 associating polymers, where shear flow breaks metastable intramolecular associations, and  
30 facilitates the formation of an intermolecular network<sup>29-31</sup>). In our case, strong flow stretches  
31 the 'bridging' strands between the stickers<sup>32,33</sup>. This stretch in turn aligns the strands at  
32 the scale of the Kuhn segments (which in water-soluble systems may disrupt the solva-  
33 tion layer<sup>7,13</sup>), so nucleating crystals as structural elements within (silk) fibres. It will turn  
34 out that such a picture contains within it a mechanism for the super-efficiency of natural  
35 silk-spinning through a surprisingly strong heterogeneity in the chain stretch distribution.

36 While this mechanism seems plausible, it is not evident how this process may be controlled  
37 and/or optimised by the number of stickers per chain and by their lifetime. Intriguingly,

38 however, it has been observed that the *Bombyx mori* silkworm tunes the sticker lifetime, and  
 39 hence the (non-)linear rheology, before and during spinning through local chemical control  
 40 variables. Prior to pupation, i.e., when the silkworm is not required to spin a cocoon, the  
 41 silk is stored in the gland at high viscosity using long sticker lifetimes<sup>8,9</sup>. When pupation  
 42 commences, potassium cations are added to decrease of the sticker lifetime and reduce the  
 43 viscosity<sup>8,9</sup>.

44 We firstly hypothesise, as schematically indicated in Fig. 1, that the decrease of the  
 45 sticker lifetime decreases the specific work needed to align the chains in the direction of the  
 46 flow field well upstream from the spinnerette. The group of Holland also discovered that  
 47 the structural features of the silk fibre are significantly enhanced through a gradient in the  
 48 pH along the spinning duct, suggesting an exquisitely controlled local rheology<sup>34</sup>. While  
 49 lower pH may induce partial folding of the protein<sup>12</sup>, it is also expected to enhance the  
 50 lifetime of the stickers. Crucially, inspired by our previous finding that broad conformational  
 51 distributions emerge due to the stochastic nature of binding and unbinding stickers<sup>10,11</sup>, we  
 52 therefore hypothesise secondly that crystallisation may be initiated by reaching a critical  
 53 concentration of highly stretched chain segments. This would require significantly less energy  
 54 input than for stretching the entire population of chain segments.

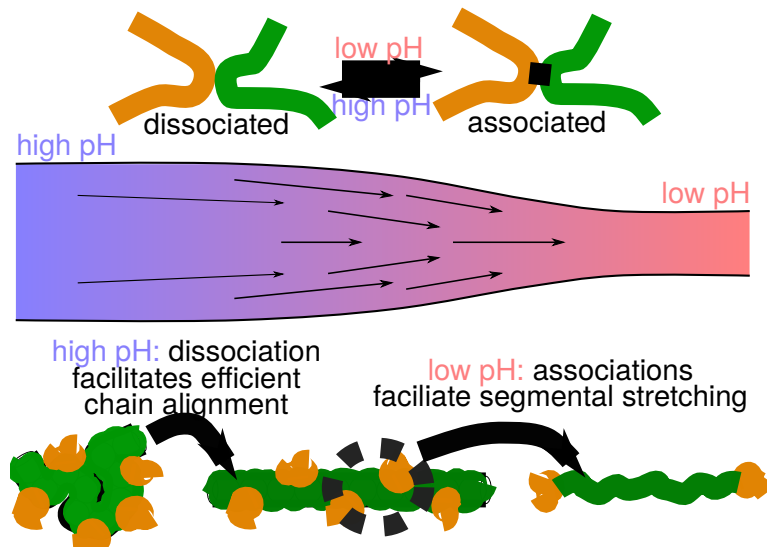
55 To theoretically investigate this hypothesis, we focus our attention on the flow-induced  
 56 preparation of the conditions for crystallisation (rather than crystallisation itself). We are  
 57 in particular interested in the specific critical work

$$W(t_s) = \int_0^{t_s} \boldsymbol{\sigma} : \boldsymbol{\kappa} dt, \quad (1)$$

58 required to induce flow-induced crystallisation after a period time  $t_s$  during which the system  
 59 is subjected to the (experimentally controllable) transpose of the (local) velocity-gradient  
 60 tensor  $\boldsymbol{\kappa} = \nabla \mathbf{v}^T$ , and the (local) stress response  $\boldsymbol{\sigma}$ . The integral is taken in the (local)  
 61 Lagrangian co-moving frame of a fluid element. In experimental works (see Ref. 35–37  
 62 and citations therein), the shear rate and duration  $t_s$  render the specific work a control  
 63 variable ( $W \approx \sigma_{xy} \dot{\gamma} t_s$ ) that controls the number of nuclei generated in the system. As the  
 64 efficiency to converse the energy input into nucleation events is rather limited (estimated  
 65  $\approx 1\%$ <sup>37</sup>), it is worth investigating how the energy loss may be reduced, e.g., by making use  
 66 of intermolecular associations.

67 Clearly, the formation of nuclei must be controlled by the underlying molecular con-

Hypothesis: chemically tunable flow processing



81 potentials. At this level of computational detail, sticker dissociation may occur following  
 82 attempts to escape the attractive potential through molecular vibrations<sup>46,47</sup>. These MD  
 83 simulations are, however, computationally very demanding, as the dissociation events are  
 84 quite rare. However, because of this rarity of events, the local equilibration of the chains  
 85 enables a much simpler description of the chain dynamics in terms of the fraction of closed  
 86 stickers,  $p$  and their lifetime,  $\tau_s$ <sup>19</sup>: In a coarse-grained picture, this sticker lifetime is an  
 87 elementary rather than an emergent timescale. This allows a description of the problem in  
 88 terms of the dynamics of a single chain in a crowded environment<sup>10,11,48–50</sup>, an approach sim-  
 89 ilar to the modelling of entangled polymers through slip-link and slip-spring models<sup>45,48,51–56</sup>,

90 where the generation and destruction of entanglements are modelled as elementary processes.  
 91 While there is no unique way of formulating a coarse-grained single-chain model<sup>57</sup>, all  
 92 variants of bead-spring, slip-link and slip-spring models can be written in the general form

$$\zeta_i \frac{\partial \mathbf{R}_i}{\partial t} = \mathbf{F}_{\text{intra},i} + \mathbf{F}_{\text{thermal},i} + \mathbf{F}_{\text{flow},i} + \mathbf{F}_{\text{network},i}, \quad (2)$$

93 where  $i$  is a chain segment at position  $\mathbf{R}_i$  that is thermally equilibrated at the relevant  
 94 time scales<sup>58</sup>. We will refer to this chain segment as a ‘node’ of an elastic network, which  
 95 may represent a non-sticky segment of a chain (a purely frictional ‘bead’), a segment with  
 96 a reversible association (a ‘sticker’), or it may be an entangled segment (a ‘slip-link’ or a  
 97 ‘slip-spring’). Which of these representations is invoked manifests itself in the definition  
 98 of the friction coefficient,  $\zeta_i$ , the (friction-dependent) thermal forces,  $\mathbf{F}_{\text{thermal},i}$ , and the  
 99 network forces,  $\mathbf{F}_{\text{network},i}$ . For instance, in classes of models where nodes move affinely with  
 100 the flow field, the network force exactly cancels the sum of the (conformation-dependent)  
 101 intramolecular force and the thermal force,  $\mathbf{F}_{\text{network},i} = -\mathbf{F}_{\text{intra},i} - \mathbf{F}_{\text{thermal},i}$ . This ‘rigid-  
 102 network approximation’ is tacitly invoked in the slip-link model by Hua and Schieber<sup>54</sup>  
 103 and in our recently published model for sticky-polymers in a rigid network<sup>10,11</sup>. Within  
 104 Likhtman’s slip-spring model, the slip-spring may diffuse within a potential energy landscape  
 105 that represents the elastic compliance of the entangled network<sup>55</sup>. In the present work, we  
 106 will account for the compliance experienced by the stickers in a reversible network.

107 In the following, in Section II A we present the usual intramolecular, thermal and drag  
 108 forces that act on single chains. To capture how the stickers modify the intermolecular  
 109 forces (i.e., the ‘elastic compliance’ of the surrounding network) and the segmental drag,  
 110 we present a non-spatially-explicit multi-chain approach. In Section II B, we present a

This is the author's peer reviewed, accepted manuscript. However, the online version of record will be different from this version once it has been copyedited and typeset.

PLEASE CITE THIS ARTICLE AS DOI: 10.1122/1.5000041

111 two-state master equation that generates analytical predictions of the impact of sticker  
112 opening and closing on both the steady-state and transient stretch distributions of the chains,  
113 which enables us to interpret our simulated data in Section III. By first mapping the results  
114 in the linear flow regime to the analytic sticky-reptation (SR) model, in Section III A we  
115 discuss how the stochastic nature of sticker opening and closing and the elastic compliance  
116 affects the linear rheological data. Then, in Section III B we show how a broad steady-  
117 state distribution of chain conformations emerges in strongly non-linear flows of shear and  
118 extension. By simulating the transient emergence of these distributions in start-up flow in  
119 Section III C, we show that the stickers initially hamper the collective alignments of the  
120 chains in mildly non-linear aligning flows, but facilitates the emergence of stretched outliers.  
121 In Section III D we discuss how these outliers may reduce the critical specific work for flow-  
122 induced crystallisation. In the discussion and conclusions of Section IV we use our findings to  
123 interpret the experimental observations of silk spinning, and argue that the chemical tuning  
124 of associations is indeed a promising mechanism to control the flow-induced crystallisation  
125 of artificial materials.

## 126 II. MODEL AND THEORY

### 127 A. Brownian dynamics of Sticky Polymers in Flow

128 In this section we will present a coarse-grained description of associating polymers, where  
129 the dynamics of sticker opening and closing will depend on the number of open and closed  
130 stickers in a non-spatially-explicit collection of chains. Any linear polymer that consists of  
131  $N$  monomers may be discretised using a number of nodes,  $N_{\text{nodes}}$ , see Fig. 2. We use the  
132 wording ‘node’ to emphasise that the node may not just represent a traditional, frictional  
133 bead of a bead-spring model, but may also represent a sticker that can be in an open or  
134 closed state, or a slip-link or slip-spring (which, unlike traditional beads, may fluctuate in  
135 numbers). Each node  $i$  is located at a spatial coordinate  $\mathbf{R}_i$  relative to the centre of mass  
136 of the chain. The strand between neighbouring nodes  $i$  and  $i + 1$  has an end-to-end vector  
137  $\mathbf{Q} = \mathbf{R}_{i+1} - \mathbf{R}_i$  and contains a fraction  $\Delta s_i = N_{s,i}/(N + 1)$  of all the monomers in the chain.

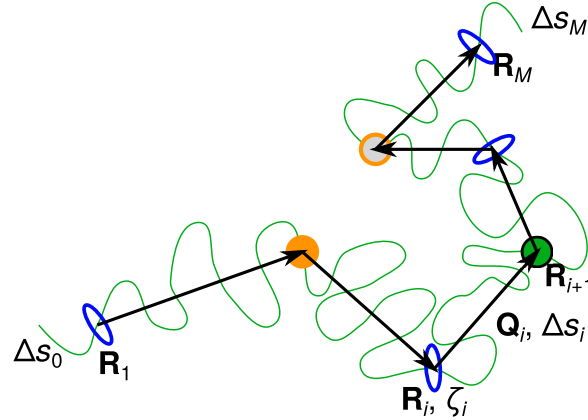


FIG. 2. The theory in Section II A applies to sticky entangled polymers that are parameterised using the locations of  $M$  nodes. Each node may be a bead (green disk), a sliplink/entanglement (blue ellipses), a closed sticker (orange disk), or an open sticker (orange circles). All nodes are assigned a friction  $\zeta_i$  that depends on the fraction of monomers of the chain,  $\Delta s_i$ , that reside in each of the  $M + 1$  substrands, see Eq. (3). In general, the number of beads and entanglements may fluctuate during a simulation. In the present work, we focus on the physics of the stickers and fix the number of beads and do not include any entanglements.

138 At this level of coarse-graining, the friction of each node is given by

$$\zeta_i = N\zeta_0 \begin{cases} \Delta s_{i-1} + \Delta s_i/2, & \text{for } i = 1 \\ (\Delta s_{i-1} + \Delta s_i)/2, & \text{for } 1 < i < N_{\text{nodes}} \\ \Delta s_{i-1}/2 + \Delta s_i, & \text{for } i = N_{\text{nodes}} \end{cases}, \quad (3)$$

139 with  $\zeta_0$  the monomeric friction. The assumption that the dangling chain ends are relaxed  
140 may be released by explicitly modelling the position of the chain ends and setting  $\Delta s_i \equiv 0$   
141 at  $i = 0$  and at  $i = N_{\text{nodes}}$ <sup>59</sup>.

142 The equilibrium structure of the chain in quiescent conditions is determined by the end-  
143 to-end distance of the substrands,  $|Q_i| = \lambda b(\Delta s_i N)^{1/2}$ , where the stretch ratio  $\lambda$  obeys the  
144 equilibrium distribution

$$P(\lambda) = 4\pi\lambda^2 (2\pi/3)^{-3/2} \exp\left(-\frac{3\lambda^2}{2}\right). \quad (4)$$

145 This distribution emerges as a consequence of the intramolecular and thermal forces in  
146 Eq. (2).

147 In order to derive the intramolecular spring forces, we consider the spring force of the  
148 entire chain of  $N$  monomers with a mean stretch ratio of unity

$$F_{\text{intra}}^{\text{strand}} = \frac{3k_{\text{B}}T}{bN^{1/2}} k_{\text{s}}(\lambda; \lambda_{\text{max}})(1 - \lambda), \quad (5)$$

149 where

$$k_{\text{s}}(\lambda; \lambda_{\text{max}}) = \frac{(3\lambda_{\text{max}}^2 - \lambda^2)/(\lambda_{\text{max}}^2 - \lambda^2)}{(3\lambda_{\text{max}}^2 - 1)/(\lambda_{\text{max}}^2 - 1)}. \quad (6)$$

150 approximately captures the anharmonicity of the spring force due to the finite extensibility  
151 of the substrand<sup>60</sup>. For the substrands  $i$  the harmonic spring force is larger than that of the  
152 full chain, and the maximum stretch ratio is smaller. This is captured by the renormalisation  
153  $F_{\text{intra}} \mapsto F_{\text{intra},i}$ ,  $N \mapsto \Delta s_i N$ , and  $\lambda_{\text{max}} \mapsto \Delta s_i^{1/2} \lambda_{\text{max}} \equiv \lambda_{\text{max},i}$ . The direction of the force  
154 exerted by spring  $i$  on node  $i$  is  $\mathbf{Q}_i/|\mathbf{Q}_i|$ , while the direction of this force acted upon node  
155  $i + 1$  is  $-\mathbf{Q}_i/|\mathbf{Q}_i|$ . Hence, the net intramolecular force exerted on node  $i$  is

$$\mathbf{F}_{\text{intra},i} = F_{\text{intra},i-1}^{\text{strand}} \frac{\mathbf{Q}_{i-1}}{|\mathbf{Q}_{i-1}|} - F_{\text{intra},i}^{\text{strand}} \frac{\mathbf{Q}_i}{|\mathbf{Q}_i|} \quad (7)$$

The thermal force is given by the equipartition theorem

$$\langle \mathbf{F}_{\text{thermal},i}(t) \rangle = \mathbf{0}; \quad (8)$$

$$\langle \mathbf{F}_{\text{thermal},i,\alpha}(t) \mathbf{F}_{\text{thermal},i,\beta}(t') \rangle = 0, \text{ for } \alpha \neq \beta \quad (9)$$

$$\langle \mathbf{F}_{\text{thermal},i,\alpha}(t) \mathbf{F}_{\text{thermal},i,\beta}(t') \rangle = 2k_{\text{B}}T \zeta_i \delta(i' - i) \delta(t' - t), \text{ for } \alpha = \beta \quad (10)$$

156 with  $\alpha, \beta = x, y, z$  the Cartesian coordinates and  $k_{\text{B}}T$  the thermal energy.

157 The force acted upon the nodes by flow is, provided that our coordinate system moves  
158 with the flow field, given by

$$\mathbf{F}_{\text{flow},i} \equiv \zeta_i \left. \frac{\partial \mathbf{R}_i}{\partial t} \right|_{\text{flow}} = \zeta_i \boldsymbol{\kappa} \cdot \mathbf{R}_i, \quad (11)$$

159 where  $\boldsymbol{\kappa}$  is the transpose of the velocity-gradient tensor, which in extension and shear is  
160 given by

$$\boldsymbol{\kappa} = \frac{1}{2} \begin{pmatrix} 2\dot{\epsilon} & 0 & 0 \\ 0 & -\dot{\epsilon} & 0 \\ 0 & 0 & -\dot{\epsilon} \end{pmatrix}, \text{ and } \boldsymbol{\kappa} = \begin{pmatrix} 0 & \dot{\gamma} & 0 \\ 0 & 0 & 0 \\ 0 & 0 & 0 \end{pmatrix}, \quad (12)$$

161 respectively. As the coordinate system moves with the flow field, the spatial quantities of  
162 physical interest to calculate are the deformation of the individual substrands

$$\left. \frac{\partial \mathbf{Q}_i}{\partial t} \right|_{\text{flow}} = \boldsymbol{\kappa} \cdot \mathbf{Q}_i, \quad (13)$$

163 using which we recursively obtain the drift of the nodes as

$$\frac{\partial \mathbf{R}_{i+1}}{\partial t} \Big|_{\text{flow}} = \frac{\partial \mathbf{Q}_i}{\partial t} \Big|_{\text{flow}} + \frac{\partial \mathbf{R}_i}{\partial t} \Big|_{\text{flow}}. \quad (14)$$

164 The value of the first entry,  $\partial \mathbf{R}_1 / \partial t$  is adjusted to fix the centre of mass of the chain (this  
165 assumes that the centre of mass moves affinely with the flow field).

166 The dynamics of the chain conformation depends on the state of the stickers through the  
167 network force, which in turn depends on the dynamics of sticker opening and closing and  
168 so, finally, on the chain conformation itself. In particular, when chain segments are highly  
169 stretched, the network forces may cause the stickers to dissociate. To obtain these forces we  
170 simulate multiple chains and track the collection of open and closed stickers. When sticker  
171  $i$  from chain A and sticker  $j$  from chain B are closed to form a pair, the friction coefficient,  
172 the thermal force, and the network force are modified until the sticker pair opens again. The  
173 friction coefficient of both nodes becomes  $\zeta_i^A + \zeta_j^B$ , where  $\zeta_i^A$  and  $\zeta_j^B$  are given by Eq. (3),  
174 and the thermal forces are given by the equipartition theorem Eq. (10) as before, but with  
175 this modified friction coefficient. The network forces are now given by

$$\mathbf{F}_{\text{network},i}^A = \mathbf{F}_{\text{intra},j}^B, \text{ and by } \mathbf{F}_{\text{network},j}^B = \mathbf{F}_{\text{intra},i}^A. \quad (15)$$

176 Hence, the paired stickers  $i$  and  $j$  have an identical friction coefficient and experience the  
177 same net force  $\mathbf{F}_{\text{intra},i}^A + \mathbf{F}_{\text{intra},j}^B + \mathbf{F}_{\text{thermal},i}^A$  (where  $\mathbf{F}_{\text{thermal},i}^A = \mathbf{F}_{\text{thermal},j}^B$ ). Crucially to forced  
178 sticker dissociation, the net force that acts on the closed sticker pair is

$$F_{\text{stic}} = |\mathbf{F}_{\text{intra},i}^A - \mathbf{F}_{\text{intra},j}^B|, \quad (16)$$

179 which we assume, as in other cases of forces temporary unbinding, lowers the activation  
180 energy for sticker dissociation as

$$E_{\text{act}} = E_{\text{act}}^0 - \ell F_{\text{stic}} \quad (17)$$

181 with  $E_{\text{act}}^0$  the activation energy in quiescent conditions and  $\ell$  the typical length scale as-  
182 sociated with sticker dissociation<sup>11</sup>. We remark that the (apparent) activation energy ob-  
183 tained from experiments using the Arrhenius-type equation<sup>24</sup>  $\tau_s = \nu^{-1} \exp(E_{\text{act}}/k_B T)$ , for  
184 the sticker lifetime with  $\nu$  an attempt frequency, may be much larger than this activation  
185 energy for dissociation. This is due to fast sticker recombination processes<sup>9,61</sup> or due to the  
186 mixing of various mechanisms of sticker opening and closing, such as bondswapping<sup>11,62</sup>.

This is the author's peer reviewed, accepted manuscript. However, the online version of record will be different from this version once it has been copyedited and typeset.

PLEASE CITE THIS ARTICLE AS DOI: 10.1122/1.5000041

187 For now, we assume a well-defined pairwise association-dissociation reaction whose equi-  
 188 librium condition is described by the detailed balance  $p/(1-p)^2 = K_0 \exp(-\ell_0 F_{\text{stic}})$ , with  $K_0$   
 189 the equilibrium constant in the absence of any chain tension. Here, the free energy  $\ell_0 F_{\text{stic}} > 0$   
 190 captures the shift in detailed balance (i.e., the fraction of closed stickers decreases with an  
 191 increasing chain tension), while  $\ell F_{\text{stic}}$  in Eq. (17) modifies the rate by which the equilibrium  
 192 is reached. Indeed, in terms of transition state theory, we may write the opening and closing  
 193 rates as  $k_{\text{open}} = \nu \exp([\theta \ell_0 F_{\text{stic}} - E_{\text{act}}^0]/k_B T)$  and  $k_{\text{close}} = \nu K_0 \exp(-[(1-\theta)\ell_0 F_{\text{stic}} + E_{\text{act}}^0]/k_B T)$ ,  
 194 respectively, where  $\ell \equiv \theta \ell_0$ , and where  $\theta \in [0, 1]$  is the so-called Brønsted-Evans-Polanyi  
 195 coefficient<sup>63</sup>. While its value may be determined using experiments or atomistic simula-  
 196 tions, we know that  $\theta$  must be larger than zero in order to capture strain-induced sticker  
 197 dissociation<sup>29-33</sup>. We argue that the rheological physics of a reversible polymer network does  
 198 not necessitate exact knowledge of  $\theta$ : When a sticker opens, it may freely diffuse and find  
 199 conditions to bind to another sticker that is not subject to the influence of strongly stretched  
 200 chain segments: association will typically take place in conditions where the activation bar-  
 201 rier is equal to that in quiescent conditions. Indeed, in our simulations we find that the  
 202 mean fraction of open stickers in conditions of strong flow remains similar to the fraction in  
 203 quiescent conditions, despite noticeable acceleration of sticker dissociation.

204 These arguments have enabled us to conveniently set  $\ell = \ell_0$  and  $\theta = 1$ ; the latter avoids  
 205 the need for on-the-fly calculations of association rates during our simulation. We have  
 206 implemented the opening and closing of stickers using a kinetic Monte Carlo (kMC; also  
 207 known as a Discrete Event Simulation) scheme, where after a time interval  $\Delta t$  a sticker is  
 208 opened or closed with a probability  $(1 - \exp[-k_{\text{open}}\Delta t])$  or  $(1 - \exp[-k_{\text{close}}\Delta t])$ , respectively.  
 209 In our simulation algorithm, shown in Fig. 3 and discussed in detail in Appendix V A, we  
 210 take time steps during which the chain conformations are approximately fixed, and for which  
 211 the time-independent (but conformation-dependent) rates of sticker opening and closing are  
 212 calculated. The dynamics of the stickers is simulated during the time step using a kMC  
 213 scheme. This essentially creates and destroys constraints in a similar way as in the slip-link  
 214 model<sup>54</sup>, but where the constraints physically represent closed stickers instead of entangle-  
 215 ments (hence, our approach may be generalised using appropriate kMC algorithms<sup>64-66</sup> to  
 216 go beyond the unentangled chains with pairwise association and dissociation of stickers fo-  
 217 cussed on in the present work, and also capture entanglements, stickers that dimerise through  
 218 bondswapping, and stickers that may assemble into larger aggregates). After this step of

219 'constraint-dynamics' the Brownian dynamics are solved, the conformations are updated,  
 220 and the next time step is commenced.

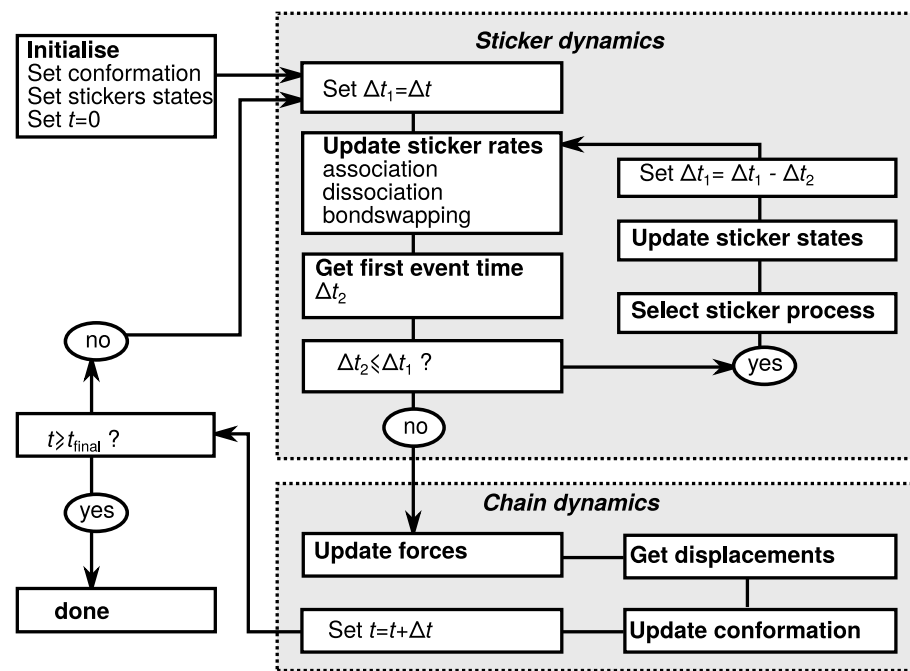


FIG. 3. Flow chart of the algorithm to simulate the conformational dynamics of sticky polymers and the dynamics of sticker association and dissociation (detailed discussion: see Appendix V A).

## 221 B. Approximate theory in transient extensional flow: Two-state model

222 The dynamics of sticky polymers is complicated by the fact that a polymer with  $Z_s$   
 223 stickers can be in  $2^{Z_s}$  different states, as each individual sticker can be either open or closed.  
 224 An instructive simple case is a chain with  $Z_s = 2$ , as the chain is either completely free to  
 225 relax when either of the stickers is open (state 1), or can only be extended by flow when  
 226 both stickers are closed (state 0). Hence, we can accurately distinguish between an extension  
 227 state where the polymer is unable to relax and a relaxation state where the polymer is able  
 228 to relax. Using this 'two-state' description, we previously discovered that stickers give rise  
 229 to enormous stretch fluctuations in extensional flow below the strain rate at which the mean  
 230 stretch diverges, i.e., below the 'stretch transition', which are described by the steady-state  
 231 power-law stretching distribution<sup>10</sup>

$$P(\lambda) \propto \lambda^\nu, \text{ with } \nu < 1, \text{ and for } \lambda \gg 1. \quad (18)$$

232 It turned out that this two-state prediction, which is exact for chains with two stickers,  
233 also described the steady-state stretch distribution for chains with multiple stickers. In the  
234 present work, we recapitulate our previous analysis of the steady-state situation and extend  
235 it for transient start-up flow. In all of this analysis we will consider a single relaxation mode  
236 of the polymer at time scales beyond the relaxation time of the surrounding network; hence,  
237 we invoke the rigid-network approximation in this entire section.

The starting point is to consider a chain in two states where the chain is either unable to retract (state 0) or is free to retract (state 1). The opening rate is  $k_{\text{open}}$  and the closing rate is  $k_{\text{close}}$ . The time development of the probability distribution of the stretch ratio is described by<sup>10</sup>

$$\frac{\partial P_0}{\partial t} = -\frac{\partial}{\partial \lambda} [\dot{\epsilon} \lambda P_0] - k_{\text{open}} P_0 + k_{\text{close}} P_1, \quad (19)$$

$$\frac{\partial P_1}{\partial t} = -\frac{\partial}{\partial \lambda} \left[ \left( \dot{\epsilon} \lambda + \frac{1-\lambda}{\tau_R} \right) P_1 \right] + k_{\text{open}} P_0 - k_{\text{close}} P_1, \quad (20)$$

with  $\tau_R$  the bare Rouse time of the chain without stickers. In this equation, we have neglected the high-frequency relaxation modes of the polymer, as well as the (potentially much slower) relaxation of the surrounding network; the latter is justified in view that the network rapidly stiffens with an increasing strain. To approximate this equation analytically, we first make the substitution  $y \equiv \ln \lambda$ , so  $\partial P_i / \partial \lambda = (1/\lambda) \partial P_i / \partial \ln \lambda \equiv \exp(-y) \partial P_i / \partial y$ . Similarly,  $\partial \lambda P_i / \partial \lambda = P_i + \partial P_i / \partial y$ . Inserting this into the governing equations gives

$$\frac{\partial P_0}{\partial t} = -\dot{\epsilon} \frac{\partial P_0}{\partial y} - (\dot{\epsilon} + k_{\text{open}}) P_0 + k_{\text{close}} P_1, \quad (21)$$

$$\frac{\partial P_1}{\partial t} = -(\dot{\epsilon} + e^{-y} - \tau_R^{-1}) \frac{\partial P_0}{\partial y} + k_{\text{open}} P_0 - (k_{\text{close}} + \dot{\epsilon} + e^{-y} - \tau_R^{-1}) P_1. \quad (22)$$

238 The non-linear contributions can then be omitted by considering the limit of large stretches  
239 where their contribution to the distribution is exponentially small, i.e., we approximate  
240  $e^{-y} \approx 0$ , which is equivalent to  $\lambda \gg 1$ .

In steady state, the left-hand side of the equation is zero and the equations can be cast in the form  $d\mathbf{P}/dy = \mathbf{A} \cdot \mathbf{P}$ , with  $\mathbf{P} = [P_0, P_1]^T$  and  $\mathbf{A}$  a constant 2 by 2 matrix. The solution of this system of first-ordinary differential equations is given by<sup>10</sup>

$$P_0^{\text{eq}} = c \lambda^\nu, \quad (23)$$

$$P_1^{\text{eq}} = \frac{k_{\text{close}}}{k_{\text{open}}} \frac{\dot{\epsilon}}{(\dot{\epsilon} - \tau_R^{-1})} P_0^{\text{eq}}, \quad (24)$$

This is the author's peer reviewed, accepted manuscript. However, the online version of record will be different from this version once it has been copyedited and typeset.

PLEASE CITE THIS ARTICLE AS DOI: 10.1122/8.0000411

241 with  $c$  a normalisation constant (its value can in principle be determined by releasing the  
 242 approximation  $e^{-y} \approx 0$ ), and with the exponent of the power-law distribution given in terms  
 243 of physical parameters by

$$\nu = -1 + \frac{k_{\text{close}}}{(\tau_{\text{R}}^{-1} - \dot{\epsilon})} - \frac{k_{\text{open}}}{\dot{\epsilon}} = -1 + \frac{1}{(1 - \dot{\epsilon}\tau_{\text{R}})} \frac{p}{(1 - p)} \frac{\tau_{\text{R}}}{\tau_{\text{s}}} - \frac{1}{\dot{\epsilon}\tau_{\text{s}}}. \quad (25)$$

244 (this is one of the eigenvalues of Eq. (21) and Eq. (22); the other eigenvalue is  $-1$  and  
 245 is unphysical as a distribution of the form  $\lambda^{-1}$  cannot be normalised.) The value of this  
 246 stretching exponent diverges if the bare stretch transition at  $\dot{\epsilon}\tau_{\text{R}} = 1$  is approached from  
 247 small strain rates. However, because of the physics of the stickers, actual divergence already  
 248 occurs at lower strain rates: At  $\dot{\epsilon}\tau_{\text{R}} = (1 - p)$ , the exponent becomes  $\nu = -1$  and the stretch  
 249 distribution can no longer be normalised. Depending on the sticker lifetime, at smaller  
 250 strain rates the exponent may reach a value  $\nu = -2$  if the ‘sticky Weissenberg number’  
 251  $(1 - p)\dot{\epsilon}\tau_{\text{R}}$  reaches unity; here, the mean stretch diverges. While the mean stretch is finite  
 252 for smaller strain rates, the variance of the stretch diverges for  $\nu \geq -3$ , which happens if  
 253  $(1 - p)\dot{\epsilon}\tau_{\text{R}}$  becomes larger than  $1/2^{10}$ , at which point (considerably slower than the bare  
 254 stretch transition) we expect a long tail of very high stretched chains to develop in the  
 255 distribution.

256 This analytic approach can be extended to predict the transient dynamics of the distri-  
 257 bution in start-up flow. As we will show, the late-stage dynamics in which the tail of the  
 258 distribution ‘fills up’ is independent of the initial conditions. In those late stages, the dis-  
 259 tribution reaches a steady state for stretches below a certain ‘front’,  $\lambda_*(t)$  (above which the  
 260 distribution function has a value of zero) which shifts to high stretch values over time. The  
 261 precise number of chains with a certain stretch also depends on the width of this moving  
 262 front. We assess analytical predictions on the front position and width using the two-state  
 263 model using solutions in an early- and late-stage regime, where the time scale is, respec-  
 264 tively, much shorter and much larger than the sticker lifetime. While the long-time regime  
 265 will slow down the progression of the front due to sticker opening, in the early-stage regime  
 266 we will obtain an upper limit of the rate by which the front moves.

267 In the early-stage regime, we approximate the stretch distribution using a the Dirac-delta  
 268 distribution (justified by the very wide long-time distribution),  $P_i(t = 0, \lambda) = c_i \delta(\lambda - \lambda_*(0))$   
 269 at  $\lambda_*(0)$ , from which it can be easily seen that the distributions shift initially, when pure  
 270 advection dominates over sticker dynamics, to higher stretches for the closed state,  $P_0(t, \lambda) =$

271  $c_0\delta(\lambda - \lambda_*(0) \exp[\dot{\epsilon}t])$  and retract to smaller stretches for the open state  $P_1(t, \lambda) = c_1\delta(\lambda -$   
 272  $\lambda_*(0) \exp[-(\tau_R^{-1} - \dot{\epsilon})t])$ . This suggests that the ‘front’,  $\lambda_*(t)$ , of any distribution with finite  
 273  $P_0$ , shifts exponentially in time to higher values through  $\lambda_*(t) = \lambda_*(0) \exp[\dot{\epsilon}t]$ .

To develop an analytic approximation for the long-time limiting behaviour of the sticky polymers in start-up flow, we consider some point in time  $t_0 \gg \tau_{SR}$  where sufficient stickers have opened to facilitate chain relaxation, and assume that the stretch distribution has reached a steady-state for small stretches  $\lambda < \lambda_*(t_0)$ , but is empty for larger stretch ratios. Here,  $\lambda_*(t_0)$  can be thought of as the establishment of the ‘front’ of the stretch distribution at later times moving to higher stretches. In the following, we will show that the ansatz of this moving front is indeed a good approximation for the tail of the transient stretch distribution and that for later times  $t > t_0$ , further convergence of the stretch distribution takes place in the range of stretches  $\lambda_*(t_0) < \lambda < \lambda_*(t)$ , where the ‘front’ of the distribution shifts to high stretch values as  $\ln[\lambda_*(t)/\lambda_*(t_0)] \propto \dot{\epsilon}(t - t_0)$ . Assuming that  $\lambda_*(t_0) \gg 1$ , the steady-state portion of the distribution is negligibly affected by the loss of small-stretch contributions to the tail of the distribution (see discussion around Eq. (51) in Appendix V B), and for any time  $t' > t_0$  the  $\lambda < \lambda_*(t')$  portion of the stretch distribution becomes independent of time beyond  $t > t'$ . The constancy of the distribution at  $\lambda_*(t_0)$  provides a fixed-boundary condition. Hence, this problem essentially models the dynamical response to a unit step, and lends itself to an analysis through a Laplace transform to give a solution for the distribution at each stretch ratio  $\lambda$  of the form  $\exp(-s\tau(\lambda))/s$ , which is the Laplace transform of a time-dependent function that becomes non-zero at the time  $\tau(\lambda)$ . The inverse function  $\lambda(\tau)$  is then the trajectory of the ‘front’ of the distribution. In Appendix V B, we detail the Laplace transform of Eqs. (21-22) with the boundary condition in this long-time regime, which as a solution gives

$$P_0(t, \lambda_*(t)) = c \left( \frac{\lambda_*(t)}{\lambda_*(t_0)} \right)^\nu \Theta(\nu' \ln[\lambda_*(t)/\lambda_*(t_0)] - \dot{\epsilon}t) \quad (26)$$

$$P_1(t, \lambda_*(t)) = \frac{k_{\text{close}}}{k_{\text{open}}} \frac{\dot{\epsilon}}{(\dot{\epsilon} - \tau_R^{-1})} P_0(t, \lambda), \quad (27)$$

274 with  $\nu$  the ‘steady-state stretch exponent’ in Eq. (25) and with

$$\nu' = \left( 1 - \frac{1}{1 - \text{Wi}} + \frac{1}{1 - \text{Wi}^{\text{sticky}}} \right) \quad (28)$$

275 the ‘dynamic stretch exponent’, which controls the growth of the front of the distribution

276 as

$$\lambda_*(t) = \lambda_*(t_0) \exp\left(\frac{\dot{\epsilon}(t - t_0)}{\nu'}\right). \quad (29)$$

277 In this equation,  $Wi = \dot{\epsilon}\tau_R$  and  $Wi^{\text{sticky}} = \dot{\epsilon}\tau_{SR}$  are the (extensional) Weissenberg numbers  
 278 of the chain without and with stickers, respectively; within the two-state model,  $\tau_{SR} = (1 -$   
 279  $p)/k_{\text{open}}$ , see discussion under Eq. (25). Upon approaching the stretch transition  $Wi^{\text{sticky}} = 1$   
 280 where the mean stretch diverges,  $\nu' \approx 0$  indicates ‘critical slowing down’, as the (late-  
 281 stage) front of the distribution becomes immobile. For chains with strong stickers  $(1 -$   
 282  $p)\tau_s \gg \tau_R$  at the strain rate  $Wi^{\text{sticky}} = 1/2$  where the variance of the stretch diverges (see  
 283 discussion under Eq. (25)), we find  $\nu' \approx 2$ , which indicates that the late-stage measure  
 284 of the front is shifted from the early-stage measure for the outliers by a factor 2. We  
 285 have also checked that the moving front is narrow for small strain rates  $Wi^{\text{sticky}} < 1/2$ .  
 286 In Appendix VB, we provide more analytical analysis of the two-state model to estimate  
 287 the width of the front (relative to its extent) as  $\Delta_{\text{rel}} \propto \sqrt{pWiWi^{\text{sticky}}/(1 - Wi^{\text{sticky}})}$ , where  
 288  $\Delta_{\text{rel}} \approx (\partial[P(\lambda, t)/P_{\text{eq}}(\lambda, \infty)]/\partial \ln \lambda)^{-1} / \ln \lambda$ . As we show in Appendix VB, typically this  
 289 width is  $\Delta_{\text{rel}} \ll 1$ , and the front of the distribution is narrow even close to the stretch  
 290 transition.

### 291 III. RESULTS

#### 292 A. Linear dynamics

293 We have verified the physics of our model in the linear viscoelastic regime by first sim-  
 294 ulating non-sticky chains of fixed length but a varying number of beads from  $M = 4$  to 64  
 295 (the beads are regularly along the backbone of the polymer, so  $\Delta s_i = 1/(M + 1)$  for all  $i$ ).  
 296 Fig. 4 shows that the choice of the number of beads has a negligible influence on the time  
 297 evolution of the mean-square displacement, MSD, of the centre of mass and is in all cases  
 298 in agreement with the theoretical prediction

$$\text{MSD} = 6Dt, \quad (30)$$

299 where the diffusivity,  $D$ , is for non-sticky polymers given by the bare Rouse diffusivity

$$D_R = \frac{1}{3\pi^2} \frac{\langle R_e \rangle^2}{\tau_R}. \quad (31)$$

300 Moreover, the inset of Fig. 4 shows that also the end-to-end-distance,  $R_e$ , is distributed  
 301 according to the physical equilibrium result of Eq. (4).

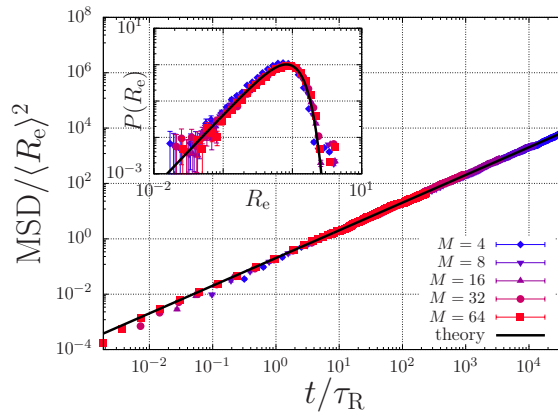


FIG. 4. Mean-square displacement, MSD, of the centre of mass of a non-sticky polymer against time (main panel) and the time-averaged end-to-end length ( $R_e$ ) distribution (inset). The number of real monomers per chain is fixed, while the level of coarse-graining is varied through varying the number of beads,  $M$ , per chain. The symbols and solid black curves represent the simulations and the theory, respectively.

302 For times shorter than the Rouse time of strands between stickers, i.e., for  $t < \tau_R(Z_s+1)^{-2}$ ,  
 303 the dynamics of a sticky polymer are governed by the same Rouse diffusion as non-sticky  
 304 chains, see Fig. 5(a). For later times than that, the motion of the polymer is subdiffusive  
 305 until the sticky Rouse time  $\tau_{SR}$ , which is approximately given by<sup>19</sup>

$$\tau_{SR} = \tau_s Z_s^2 \left( 1 - \frac{9}{p} + \frac{12}{p^2} \right)^{-1}. \quad (32)$$

306 Focussing on the crossover from early-stage bare Rouse diffusion to subdiffusive motion, one  
 307 would expect this crossover to occur at the point in time where the substrands between  
 308 stickers have just relaxed, and where further relaxation requires sticker dissociation. Indeed,  
 309 we find this is the case within the rigid-network approximation. However, for the elastically  
 310 compliant network the closed stickers themselves are able to diffuse. The friction experienced  
 311 by the closed sticker depends on the level of deformation of the surrounding network, which  
 312 is initially small. As the sticker diffuses further, a larger portion of the surrounding network  
 313 is deformed and the contribution of ‘next-neighbour’ stickers starts to contribute to the  
 314 friction. Clearly, the increase of the friction increases rapidly beyond a certain characteristic

This is the author's peer reviewed, accepted manuscript. However, the online version of record will be different from this version once it has been copyedited and typeset.

PLEASE CITE THIS ARTICLE AS DOI: 10.1122/8.0000411

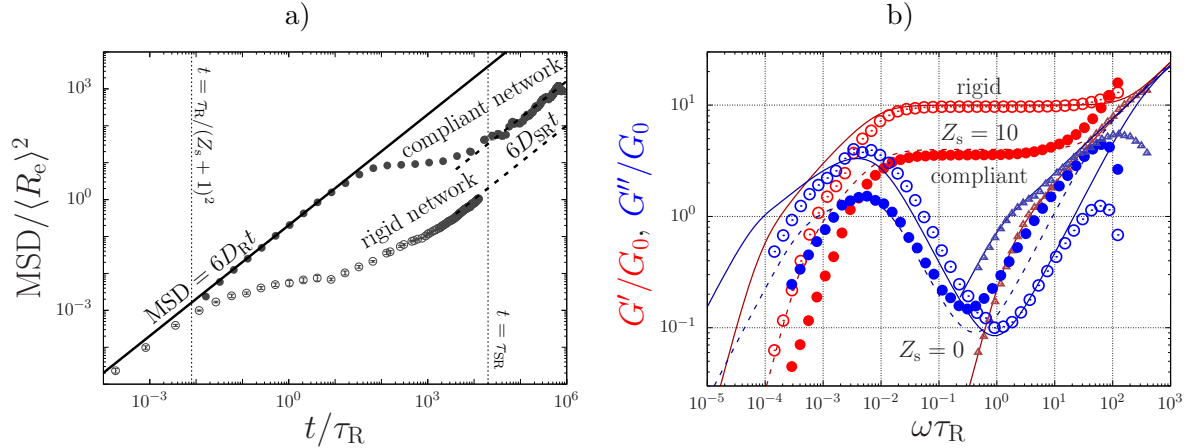


FIG. 5. Linear rheology of a sticky chain with  $Z_s = 10$ ,  $p = 0.9$ ,  $\tau_s = 200\tau_R$  within the rigid-network approximation (open symbols) and with this approximation released (closed symbols). (a) Mean-square displacement MSD of the centre of mass against time. (b) Storage,  $G'$ , and loss,  $G''$ , modulus in units of  $G_0$  against the frequency,  $\omega$ , plotted for the chain in (a) as well as for a non-sticky chain (triangles). There is fair agreement with the analytical sticky-Rouse model in Eq. (33) (solid curves) for the sticky chain within the rigid-network approximation and for the non-sticky chain. For the sticky chain with an elastically compliant network the plateau modulus decreases to that of the theory with  $Z_s = 4$  (dashed curves).

315 distance. It is unknown what this distance might be, but it is likely to be strongly dependent  
 316 on the topology of the network. The plateau value in Fig. 5(a) shows that for our simulations  
 317 this happens to occur when the MSD of the centre of mass of chain is approximately 10,  
 318 i.e., when the centre of mass of the chain has diffused 3 – 4 times its end-to-end distance.

319 The elastic compliance not only affects the subdiffusive motion of the chain, but also the  
 320 sticky Rouse diffusivity  $D_{SR} = D_R\tau_R/\tau_{SR}$  at times beyond the sticky Rouse time. While  
 321 the analytical expression for the sticky Rouse diffusivity accurately describes our simulations  
 322 within the rigid-network approximation, we find that it overestimates the diffusivity of chains  
 323 in an elastically compliant network. We have investigated the consequence of this to the  
 324 interpretation of linear viscoelastic data, which are often used experimentally to estimate  
 325 the number of associations per chain, by calculating the dynamic moduli  $G'$  and  $G''$  against  
 326 the frequency  $\omega$  in Fig. 5(b). The data shown includes non-associating unentangled chains  
 327 ( $Z_s = 0$ ) and the unentangled sticky chains of Fig. 5(a); i.e., chains with  $Z_s = 10$  stickers  
 328 within the rigid-network approximation and with an elastically compliant network. The

329 simulated data (symbols) were obtained from the relaxation modulus,  $G(t)$ , through the  
 330 multiple-tau-correlator algorithm discussed in Ref.<sup>67</sup>. To obtain the dynamic moduli  $G'$   
 331 and  $G''$  we have used the finite-element approach from Ref.<sup>68</sup>. We have compared the data  
 332 to the sticky-Rouse model (curves), which is given by

$$G(t) = G_0 \sum_{p=Z_s+1}^N \exp\left(-\frac{2p^2t}{\tau_R}\right) + G_0 \sum_{p=1}^{Z_s} \exp\left(-\frac{2p^2t}{\tau_s Z_s^2}\right). \quad (33)$$

333 In this equation, the first summation captures the high-frequency bare Rouse modes (the  
 334 number of Kuhn segments,  $N$ , truncates the highest frequencies), and the second summation  
 335 captures the sticky Rouse modes. The modulus  $G_0$  is proportional to the number density of  
 336 monomers and to the thermal energy.

337 Fig. 5(b) shows dominance of bare Rouse relaxation at high frequencies, where all moduli  
 338 will approach (in principle) the scaling relation  $G', G'' \propto \omega^{1/2}$ . Discrepancies, such as a  
 339 roll-off of  $G''$  at high frequencies, emerge due to the finite number of modes/beads that are  
 340 included in the simulations. At decreasing frequencies the moduli of the non-sticky chains  
 341 (triangles) decrease rapidly, while the moduli of the sticky chains reach a plateau value  
 342 that ranges down to  $\omega = 1/\tau_s$ . Within the rigid-network approximation (closed circles),  
 343 the modulus of the plateau is  $G'(\omega) = G_0 Z_s$  in agreement with the sticky-Rouse model in  
 344 Eq. (33) for  $Z_s = 10$ . However, if the network is elastically compliant (open circles), the  
 345 plateau value decreases and is better described if the theory would be adjusted with an  
 346 apparent number of stickers  $Z_s = 4$  (dashed curves). At lower frequencies  $\omega < 1/\tau_s$  the  
 347 moduli rapidly decrease. In the simulations the moduli decrease much more rapidly than in  
 348 the theory, as also noted earlier in Ref. 50. We find that this terminal relaxation time (we  
 349 remind the reader that this relaxation time is for unentangled chains entirely determined  
 350 by sticker relaxation, i.e., not by sticky reptation<sup>22,24</sup>) is even further reduced for the chain  
 351 in an elastically compliant network. Consequently, the peak of the dynamic modulus  $G''$  is  
 352 much narrower than in the theory. We have estimated that the shape of this peak is best  
 353 described by  $Z_s = 4$  within the rigid-network approximation and  $Z_s = 3$  for the compliant  
 354 network. This clearly indicates that analysis of the dynamic modulus peak in rheological  
 355 data (which is required when high frequencies are experimentally inaccessible<sup>9</sup>) provides an  
 356 underestimate of the actual number of stickers per chain.

357 To obtain a wider view of the impact of the elastic compliance on the dynamics of chains  
 358 with a various number of stickers and sticker lifetimes, we have calculated the diffusivities

This is the author's peer reviewed, accepted manuscript. However, the online version of record will be different from this version once it has been copyedited and typeset.

PLEASE CITE THIS ARTICLE AS DOI: 10.1122/8.0000411

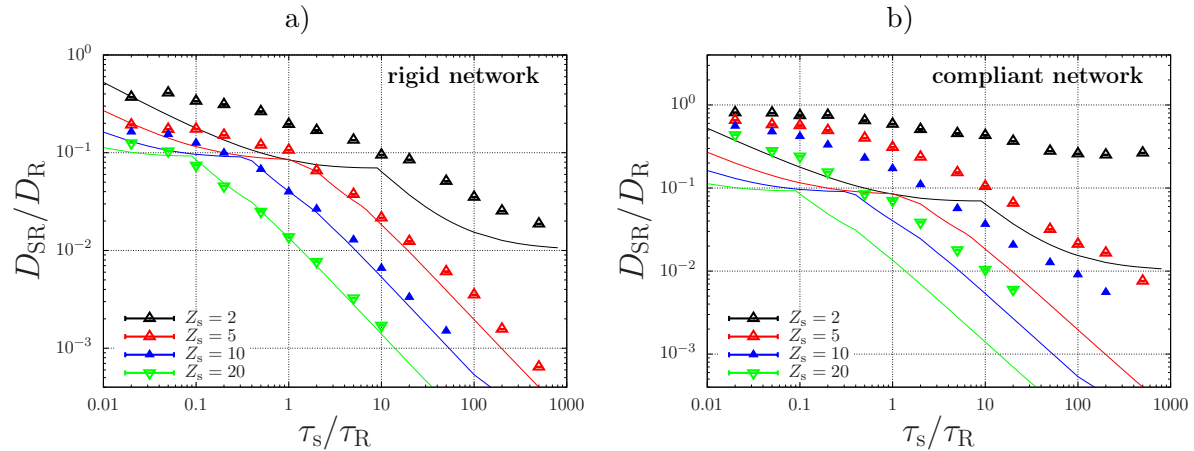


FIG. 6. Sticky Rouse diffusivity,  $D_{SR}$ , against the sticker lifetime,  $\tau_s$  for chains with  $Z_s = 2, 5, 10, 20$  stickers with  $p = 0.9$  within a rigid network (a) and a compliant one (b). The symbols are our simulation results, and the curves represents the sticky Rouse model in Ref.<sup>19</sup>. The units are given in terms of the bare Rouse diffusivity  $D_R$  and the bare Rouse time,  $\tau_R$ .

359 of various chains within the rigid-network approximation and with a compliant network  
 360 in Fig. 6. Panel (a) shows that the predictions of Ref.<sup>19</sup> describes our simulations well  
 361 within the rigid-network approximation for chains with 5, 10, 20 stickers with various sticker  
 362 lifetimes, in particular in the regime where the sticky-Rouse diffusivity scales with the sticker  
 363 lifetime as  $D_{SR} = D_R \tau_R / \tau_{SR} \propto 1 / \tau_s Z_s^2$ , see Eq. (32). Panel (b) shows that upon releasing the  
 364 rigid-network approximation this scaling behaviour persists, but rescaled with a prefactor  
 365  $\approx 4$ . While this scaling regime is reached for the chains with more than 5 stickers (i.e., above  
 366 the percolation threshold for network formation), this is not the case for the chains with 2  
 367 stickers. Within the rigid-network approximation, this originates from the fact that at sticker  
 368 lifetimes a plateau is reached where the chains with all stickers open dominate the dynamics.  
 369 Without the rigid-network approximation, the chains cluster into linear ‘supramolecular’  
 370 dimers, trimers, etc. through an exponentially decaying cluster-size distribution<sup>69</sup>, which  
 371 implies a distribution of diffusivities that strongly differs from that predicted by the sticky-  
 372 Rouse model. Hence, while our simulation approach accounts for the elastic compliance  
 373 of the percolating network, it also captures the contributions of cluster diffusion near and  
 374 below the percolation threshold for network formation.

375 **B. Non-Linear Dynamics: Steady State**

376 Ordinary Gaussian polymer melts and solutions of narrow molecular-weight distribution  
 377 exhibit broad conformational distributions in shear flow due to dynamic stretching, tumbling  
 378 and recoiling of the chains<sup>40–42</sup>. In extensional flow, however, such chains do not tumble and  
 379 recoil, and their stretch distributions are narrow, see Fig. 7(a). Perhaps surprisingly, by  
 380 incorporating stickers into the chain these stretch distributions become much wider, see  
 381 Fig. 7(b). This figure shows that the sticky chains exhibit an enormous dispersity in the  
 382 chain stretch, as well as occasional hairpin conformations (Fig. 7(b)). These are caused by  
 383 the stochastic binding and unbinding of stickers, where the network forces may occasionally  
 384 act in the opposite direction of the drag forces exerted by flow.

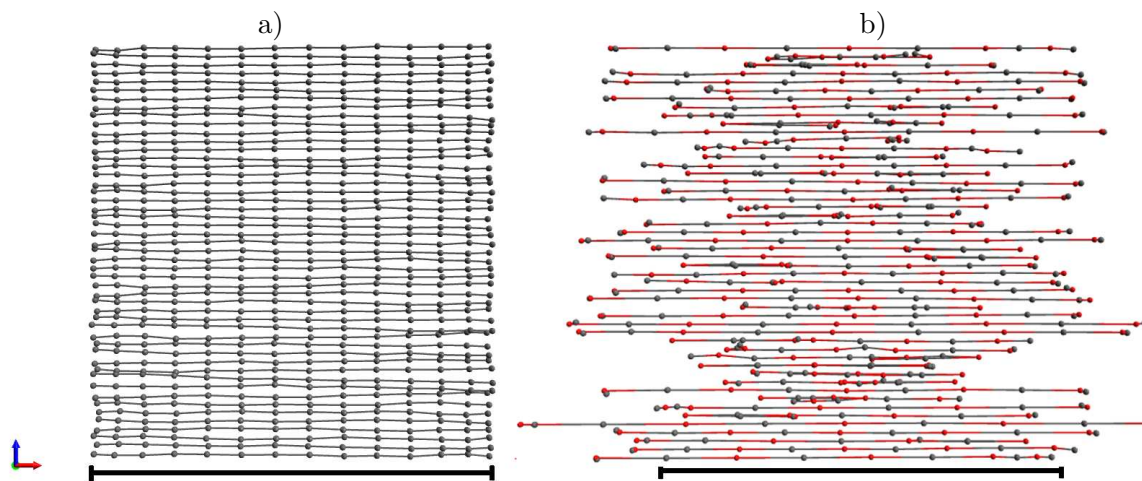


FIG. 7. Representation of simulated chain conformations in extensional flow for  $\dot{\epsilon}\tau_R = 2$  for non-sticky (a) and sticky (b) polymers. While the variations in stretch are narrow for non-sticky polymers, these variations are broad for the sticky polymers: when a sticker in a retracting chain segment binds to a neighbouring chain segment, this may disrupt the neighbouring chain. The scale bar represents approximately a length  $50R_e$ , which is 65% of the fully extended chain.

385 To go beyond these qualitative observations, we have quantified this phenomenon using  
 386 steady-state stretch distributions of polymers at various extension and shear rates in Fig. 8.  
 387 We have selected non-sticky polymers ( $Z_s = 0$ ), and sticky polymers below ( $Z_s = 2$ ) and  
 388 above ( $Z_s = 5$ ) the percolation threshold for network formation: The chains with only 2  
 389 stickers may only assemble into high-molecular weight chains, while chains with 5 stickers  
 390 may branch into percolating networks. We have modelled the physics of the stickers using

391 the same description as in our previous work on chains that are pre-aligned in the flow  
 392 field<sup>11</sup>. We have summarised the associated parametrisation in the caption of Table I. In  
 393 extensional flow, above the sticky Weissenberg number,  $Wi^{\text{sticky}} = \dot{\epsilon}\tau_{\text{SR}}$  with  $\tau_{\text{SR}}$  the sticky  
 394 Rouse time we expect divergent stretching (albeit that real divergence is obstructed by the  
 395 maximum chain extensibility  $\lambda_{\text{max}} = 75$ ). We have calculated the sticky Rouse time as  
 396  $\tau_{\text{SR}} = [D_{\text{R}}/D_{\text{SR}}]\tau_{\text{R}}$ , with the ratio between the sticky and the bare diffusivity as presented  
 397 above in Fig. 6. The relevant results are summarised in Table I.

TABLE I. In our simulations of sticky polymers in non-linear flow conditions we use as parameters  
 $p = 0.9$  as the fraction of closed stickers (in quiescent conditions), a sticker lifetime  $\tau_s = 10\tau_{\text{R}}$ ,  
 an activation energy  $E_{\text{act}} = 8k_{\text{B}}T$ , and a sticker dissociation length of  $\ell = 1$  nm. The maximum  
 extension ratio of the chain is  $\lambda_{\text{max}} = 75$ . The intramolecular forces in Eq. 5 are calculated by  
 assuming a total number of  $N = 5525$  Kuhn segments, and a Kuhn length of  $b = 0.4$  nm. As we  
 focus on chains with  $Z_s = 2$  and 5 stickers, we here tabulate the ratio between the bare Rouse  
 and sticky Rouse diffusivities,  $[D_{\text{R}}/D_{\text{SR}}]$ , and relaxation times,  $[\tau_{\text{R}}/\tau_{\text{SR}}]$ . The diffusivities were  
 determined in Fig. 6, and the sticky Rouse time is calculated as  $\tau_{\text{SR}} = [D_{\text{R}}/D_{\text{SR}}]\tau_{\text{R}}$ <sup>19</sup>.

Polymer model	$D_{\text{SR}}/D_{\text{R}}$	$\tau_{\text{SR}}/\tau_{\text{R}}$
$Z_s = 2$ ; (rigid)	$0.0949 \pm 0.0002$	$10.54 \pm 0.02$
$Z_s = 5$ ; (rigid)	$0.02156 \pm 0.00004$	$46.38 \pm 0.09$
$Z_s = 2$ ; (compliant)	$0.4331 \pm 0.001$	$2.309 \pm 0.005$
$Z_s = 5$ ; (compliant)	$0.1050 \pm 0.0002$	$9.52 \pm 0.02$

398 Eq. (4) shows that in all cases the equilibrium stretch distribution for zero-flow conditions  
 399 (black curve) is approached for small strain rates. For non-sticky chains ( $Z_s = 0$ ), a broad  
 400 stretch distribution with a cutoff set by  $\lambda_{\text{max}}$  emerges in shear due to the dynamic stretching,  
 401 tumbling and re-collapsing of the chains. In extensional flow, the distribution broadens only  
 402 within a narrow range of strain rates  $0.9 < \dot{\epsilon}\tau_{\text{R}} < 1.1$  around the bare stretch transition,  
 403  $Wi = \dot{\epsilon}\tau_{\text{R}} = 1$ . Beyond the stretch transition, the stretch distribution is narrow and Gaussian  
 404 and approaches  $\lambda_{\text{max}}$  with an increasing strain rate. This behaviour qualitatively changes  
 405 upon incorporating stickers.

406 Fig. 8 shows that the steady-state stretch distributions in shear are similar to those of the  
 407 non-sticky chains, while in extensional flow the distributions of sticky polymers are remark-

This is the author's peer reviewed, accepted manuscript. However, the online version of record will be different from this version once it has been copyedited and typeset.

PLEASE CITE THIS ARTICLE AS DOI: 10.1122/8.0000411

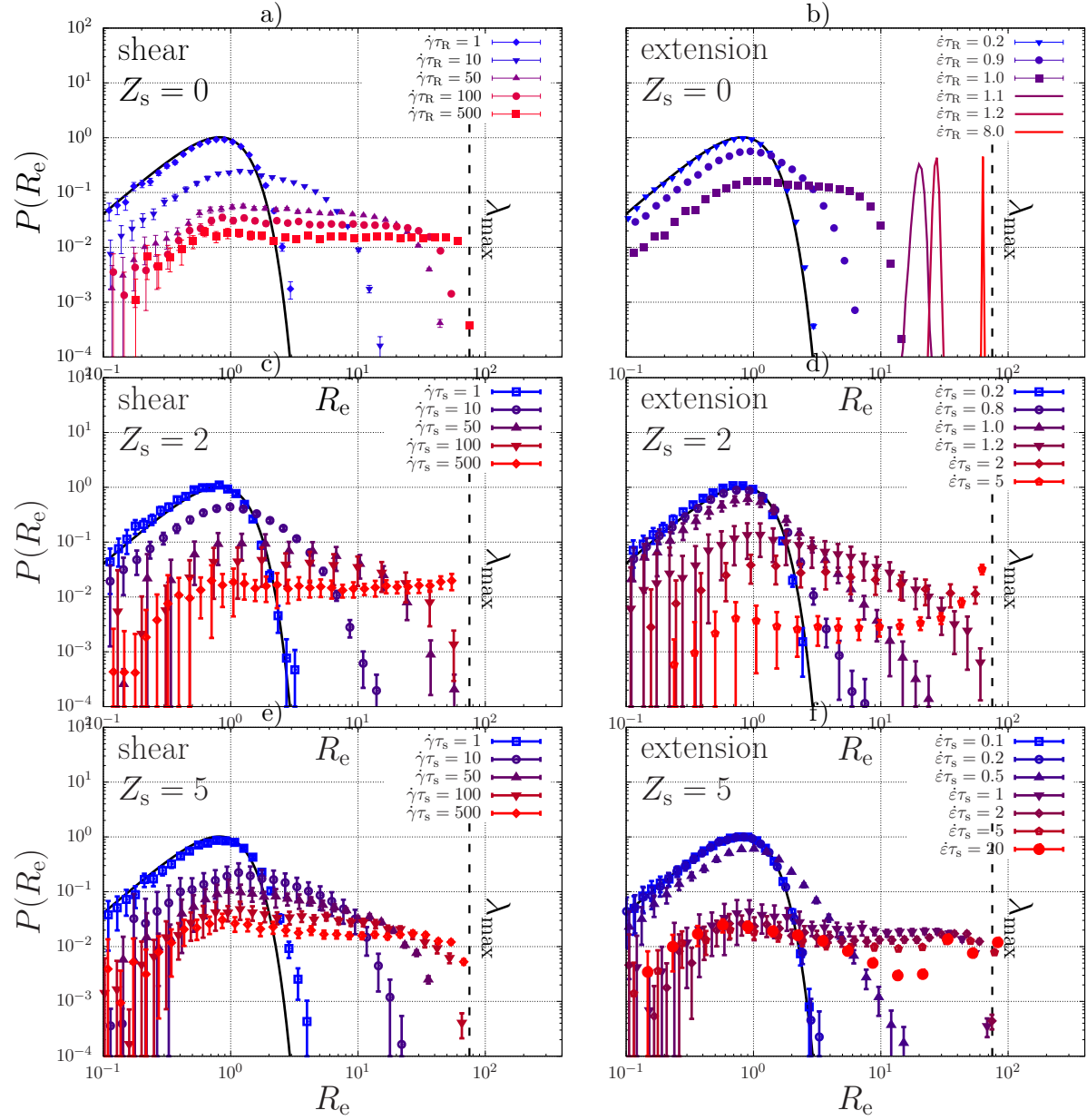


FIG. 8. Simulated steady-state stretch distributions of the end-to-end distance,  $R_e$ , for various extension (a,c,e) and shear (b,d,f) rates for a linear unentangled, non-sticky ( $Z_s = 0$ ) and sticky ( $Z_s = 2$  and  $Z_s = 5$ ) polymers. For these simulations  $\tau_{SR} \approx \tau_s = 10\tau_R$  (see Table I for all parameter values). The black curve represents the contour-length fluctuations in quiescent conditions, given by Eq. (4).

ably distinct from the non-sticky ones: In contrast to the non-sticky polymers, the sticky  
 polymers show broad stretch distributions in steady-state extensional flow over a broad range  
 of flow rates. We have observed this behaviour previously in simulations where the chains

This is the author's peer reviewed, accepted manuscript. However, the online version of record will be different from this version once it has been copyedited and typeset.

PLEASE CITE THIS ARTICLE AS DOI: 10.1122/8.0000411

411 were pre-aligned in the flow-field and where we invoked the rigid-network approximation<sup>11</sup>.  
 412 Our current simulations show that this phenomenon persists when these approximations are  
 413 released, but also show a dynamic coexistence of stretched chains, relaxed coils, and hairpins.  
 414 Interestingly, there is a qualitative similarity between the distributions of the chains with 2  
 415 or 5 stickers, despite the fact that these are below and above the percolation threshold for  
 416 network formation, respectively. This indicates that the enormous reduction of the chain  
 417 retraction rate due to the stickers does not necessitate network formation: the formation of  
 418 high-molecular weight assemblies suffices.

419 We also find that the large fluctuations in stretch below the formal stretch transition  
 420 carry over from case of 2 stickers per chain to multiple stickers<sup>11</sup>. (The stretch transition is  
 421 defined at the condition  $\dot{\epsilon}\tau_{\text{SR}} = 1$ , with the sticky Rouse time obtained from the sticky-Rouse  
 422 diffusivity of Fig. 6 as  $\tau_{\text{SR}} = \tau_{\text{R}}D_{\text{SR}}/D_{\text{R}}$ ) In particular, we find that for small strain rates and  
 423 large stretch ratios  $\lambda$  the stretch distribution has a power-law tail (see Eq. (18)) of which the  
 424 width is set by a  $\dot{\epsilon}$ -dependent stretch exponent  $\nu$  (see Section II B). We have determined the  
 425 stretch exponent from the distributions of the chains with 2 and 5 stickers (we discuss the  
 426 numerical method in Appendix V C) in extensional flow with and without the rigid-network  
 427 approximation and finite extensibility, and plot these against the strain rate in Fig. 9. As  
 428 anticipated, we have been able to map the stretch exponent of the chain with two stickers  
 429 onto the analytical result in Eq. (25). To achieve that, it has to be taken into account that  
 430 the open state of the chain can be achieved by opening either of the stickers; hence,  $\tau_{\text{s}}$  in  
 431 Eq. (25), which models the simultaneous opening of all stickers, is replaced by  $\tau_{\text{s}}/2$ , and  
 432 results in

$$\nu = -1 - \frac{1}{(1 - \dot{\epsilon}\tau_{\text{R}})} \frac{p}{(1 - p)} \frac{2\tau_{\text{R}}}{\tau_{\text{s}}} + \frac{2}{\dot{\epsilon}\tau_{\text{s}}}. \quad (34)$$

433 For chains with multiple stickers, no such analytic theory is yet available; however, we do  
 434 find a qualitative agreement of the increasing power-law exponent with an increasing strain  
 435 rate.

436 For the chains with 2 and 5 stickers and with a fraction  $p = 0.9$  of closed stickers, we  
 437 also simulated the stretch distributions while including finite extensibility and an elastically  
 438 compliant network. Finite extensibility implies that there is a cutoff of the power-law tail,  
 439 which becomes apparent with increasing (less negative)  $\nu$ . Since the fluctuations in  $\lambda$  diverge  
 440 for  $\nu \geq -3$ , this cutoff has a significant effect on the tail of the stretch distribution upon  
 441 approaching  $\nu = -3$ . Fig. 9 does confirm a broadening power-law stretch distribution for

This is the author's peer reviewed, accepted manuscript. However, the online version of record will be different from this version once it has been copyedited and typeset.

PLEASE CITE THIS ARTICLE AS DOI: 10.1122/8.0000411

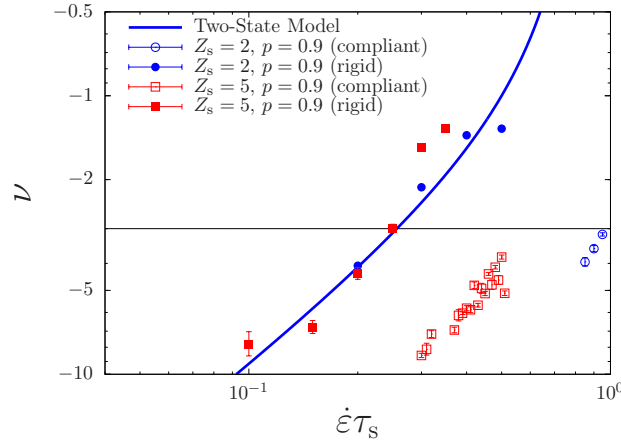


FIG. 9. Stretch exponent  $\nu$  of the power-law tail of the stretch distribution  $P \propto \lambda^\nu$  for simulations of polymers with  $Z_s = 2$  (blue symbols) and 5 stickers (red symbols), within the rigid-network approximation (closed symbols) and using elastic compliance and finite chain extensibility (open symbols). The solid curve is given by the two-state model in Eq. (34) with  $\tau_s = 10\tau_R$  (see Table I for all physical parameter values). For  $\nu > -3$  (horizontal line) the fluctuations in stretch diverge; this leads to a cutoff in the stretch distribution for chains with finite extensibility, see Fig. 8.

442 the chains in a compliant network, but shifted to higher strain rates, as expected from the  
443 faster sticky-diffusion rates from Fig. 4.

### 444 C. Non-Linear Dynamics: Transients

445 In our pursuit to understand the flow-induced crystallisation of associating polymers such  
446 as the silk protein, we are interested in capturing the macroscopically observable stresses in  
447 start-up flow, and to interpret crystallisation rates in terms of the chain conformations that  
448 underlie these stresses. To address these challenges, in this section we will present the time-  
449 dependent rate-normalised transient shear stress,  $\sigma_{xy}/\dot{\gamma}$ , and extensional stress  $(\sigma_{yy} - \sigma_{rr})/\dot{\epsilon}$ ,  
450 with the stress tensor (in units of energy per molecule) given by

$$\sigma_{\alpha\beta} = \frac{3k_B T}{b^2 N} \sum_{i=1} \Delta s_{i-1} k_{s,i} \frac{Q_{\alpha,i}}{\Delta s_{i-1}} \frac{Q_{\beta,i}}{\Delta s_{i-1}}. \quad (35)$$

451 Focussing first on the results for non-sticky chains with a finite extensibility  $\lambda_{\max} = 75$  in  
452 Fig. 10(a,b), we reproduce the well-known qualitative features of their stress transient<sup>57</sup>: For  
453 small Weissenberg numbers,  $\dot{\epsilon}\tau_R < 1$ ,  $\dot{\gamma}\tau_R < 1$  the polymers are able to relax, while for large

This is the author's peer reviewed, accepted manuscript. However, the online version of record will be different from this version once it has been copyedited and typeset.

PLEASE CITE THIS ARTICLE AS DOI: 10.1122/8.0000411

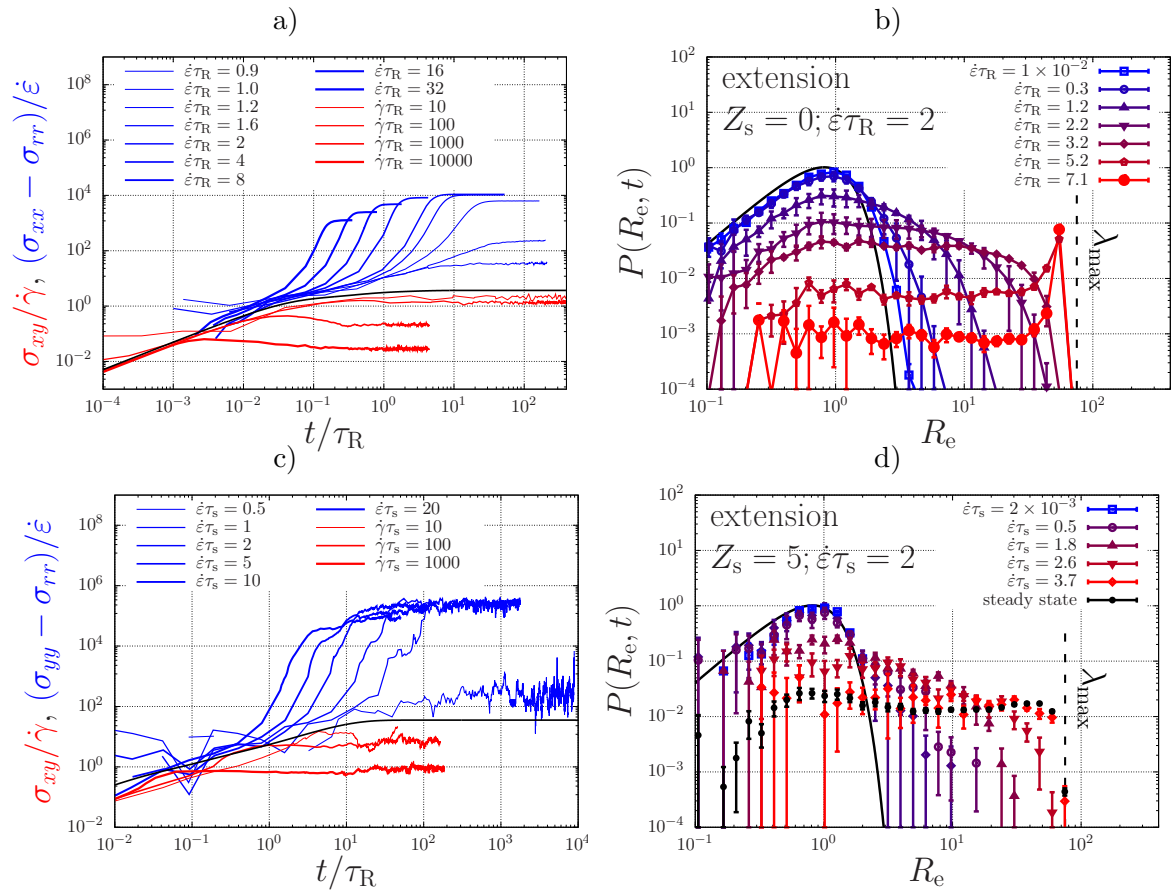


FIG. 10. (a,c) Simulated rate-normalised transient extensional and shear stresses averaged over 50 polymers the non-sticky (a) and the sticky (c) case. The sticky polymer exhibits strong fluctuations for  $\dot{\epsilon}\tau_s = 0.5$ , which is below the stretch transition (at  $\dot{\epsilon}\tau_s \approx 1$ , see Table I). (b,d) Transient stretch distribution of the end-to-end distance,  $R_e$ , in extensional flow for the non-sticky (b) and sticky (d) chain at selected strain rates. The error bars in (d) represent half of the standard error of the mean. All physical parameter values are given in Table I.

454 strain rates there is an overshoot in shear flow, which is related to the onset of tumbling  
 455 and re-collapsing of stretched chains, and in extensional flow there is a sharp increase in the  
 456 extensional stress until a plateau due to the finite extensibility of the chains is reached. Be-  
 457 cause of the thermal fluctuations and dispersity in the initial chain conformations, Fig. 10(b)  
 458 shows broadening of the stretch distribution at early times. At late times, when all chains  
 459 are aligned (at the level of the beads), a sharp peak emerges at high stretches near the  
 460 maximum extensibility  $\lambda_{max}$ .

461 This sharp peak in the stretch distribution is a fingerprint for non-sticky linear polymers

462 in extensional flow, and will not be visible for the sticky polymers, as we we will now show  
 463 for  $Z_s = 5$ . We plot the resulting start-up stresses and stretch distributions in Fig. 10(c,d).

464 Qualitatively, we find similar shear and extensional viscosities as in the non-sticky case,  
 465 although there is now no distinctive overshoot in shear flow. In extensional flow, the stresses  
 466 at long time scales have shifted to higher values because of the contribution by the reversible  
 467 cross-links. Further, while non-sticky polymers show strain hardening only for  $\dot{\epsilon}\tau_R > 1$ ,  
 468 the sticky ones also show strain hardening for smaller strain rates  $\dot{\epsilon}\tau_s > 1$ . For strain  
 469 rates smaller than that we identify large fluctuations in the transient extensional stress,  
 470 which are caused by temporary exponential stretching of chain segments between closed  
 471 stickers that rapidly retract to a near-relaxed state when the stickers open<sup>10</sup>. For strain rates  
 472  $0.3 < \dot{\epsilon}\tau_s < 0.5$  these fluctuations fill up a power-law distribution whose stretch exponent is  
 473 depicted in Fig. 9. For higher rates, the finite extensibility causes a truncation of this power  
 474 law tail.

475 The dynamics by which the stretch distributions evolve in extensional flow above the  
 476 stretch transition ( $\dot{\epsilon}\tau_s = 2$ ) is shown in Fig. 10(d). At early times, the stretch distribution  
 477 closely resembles the equilibrium distribution of Eq. (4). As time proceeds, a the distribution  
 478 broadens exponentially with time as  $\ln \lambda \propto \dot{\epsilon}t$  until the steady state is reached after a time  
 479  $\dot{\epsilon}\tau \propto \ln \lambda_{\max}$ . This is in qualitative agreement with the predictions of the two-state model  
 480 that we derived in Eq. (29) of Section II B.

#### 481 D. Critical specific work

482 Now that we have captured how stickers lead to broad stretch distributions, we will  
 483 investigate how these distributions affect the critical work for flow-induced crystallisation  
 484 (FIC). The usual predictor for FIC is the ‘Kuhn segment nematic order parameter’,  $P_{2,K} \in$   
 485  $[0, 1]$ . If  $P_{2,K} \rightarrow 1$  (see e.g. Ref. 3), virtually all chains are aligned at the level of the  
 486 Kuhn segments, i.e., they are completely extended/stretched in the direction of the flow  
 487 field. However, in this case of high chain-heterogeneity we expect this average measure  
 488 to be a poor descriptor. We know that the critical nuclei will be dominated by the small  
 489 fraction of highly-stretched chains, and that it is the oriented segments in these chains  
 490 only that promote crystallisation. To model this extremum-dominated physics, therefore,  
 491 we will assume that FIC may commence when a critical fraction,  $P_s$ , of chain segments

492 of some length  $\Delta s^* \in [0, 1]$ , have stretched beyond a critical stretch ratio  $L_s \lambda_{\max}^*$ , where  
 493  $\lambda_{\max}^* = \lambda_{\max} \sqrt{\Delta s^*}$  is the maximum stretch of the chain segment and  $L_s^* \in [0, 1]$  a parameter  
 494 that may be viewed as proxy for chain stretch at the Kuhn length of this extremely stretched  
 495 chain fraction. Hence, the criterion for FIC may within our interpretation be formulated as

$$\int_{L_s \lambda_{\max}^*}^{\lambda_{\max}^*} P(\lambda, t_s) d\lambda \geq P_s, \quad (36)$$

497 where  $P(\cdot)$  is the transient stretch distribution function, and  $t_s$  is the time into the process  
 498 of startup flow at which the criterion is satisfied. Essentially, this criterion provides a pre-  
 499 diction for the time required to form the first nuclei, and, hence the time  $t_s$  should not be  
 500 confused with the fixed time in FIC experiments<sup>35-37</sup> during which a different number of  
 501 nuclei may form depending on the strain rate. A comparison to those experiments would  
 502 require knowledge of the physical relationship between the nucleation rate and the conforma-  
 503 tional distribution; here, we have proposed a hypothetical condition that is likely to correlate  
 504 to a fixed nucleation rate. For associating polymers, a natural measure for the length of  
 505 flow-crystallisable chain segments is  $\Delta s^* = 1/(Z_s + 1)$ ; in general, however, measures for  
 506  $P_s$ ,  $L_s$ , and  $\Delta s^*$  will have to be determined through experimentation and (atomistic) MD  
 507 simulations<sup>15-18</sup>.

508 In this section, we will employ simulations with 50 chains of a fixed number of 11 beads  
 509 (i.e., with 10 chain segments, giving  $\Delta s^* = 1/10$ ), and we will monitor the maximum  
 510 stretch among the total of 500 chain segments (i.e.,  $P_s = 1/500$ ). The time-evolution of  
 511 the maximum stretch will enable us to screen how various values of  $L_s$  require a different  
 512 processing time  $t_s$  and a different input of specific energy. We obtain statistics on this  
 513 relationship by averaging our results over 5 simulations with different initialisation 'seeds' of  
 514 the random-number generator. We will discuss the implications of the criterion in Eq. (36)  
 515 by comparing it to a measure of the (mean-field-type) nematic order parameter. At our  
 516 level of coarse graining, the highest resolution of nematic chain alignment is captured using  
 517 the nematic order parameter  $P_{2,s} \in [0, 1]$ , which is the largest eigenvalue of the nematic  
 518 order tensor  $\mathbf{P}_{2,s} = (3\langle \mathbf{u}\mathbf{u} \rangle - 1)/2$ , where  $\mathbf{u}$  is the unit vector tangential to the backbone of  
 519 the chain. (we remark that this nematic order parameter is an overestimate of the Kuhn  
 520 segment nematic order, i.e.,  $P_{2,s} > P_{2,K}$ ) In Fig. 11, we have calculated the critical specific  
 521 work,  $W$ , as given in Eq. (1), needed to achieve values of  $P_{2,s}$  and  $L_s$  in the range from 0 to

This is the author's peer reviewed, accepted manuscript. However, the online version of record will be different from this version once it has been copyedited and typeset.

PLEASE CITE THIS ARTICLE AS DOI: 10.1122/8.0000411

522 1 for non-sticky ( $Z_s = 0$ ) and sticky ( $Z_s = 5$ ) chains for various shear and extensional rates.

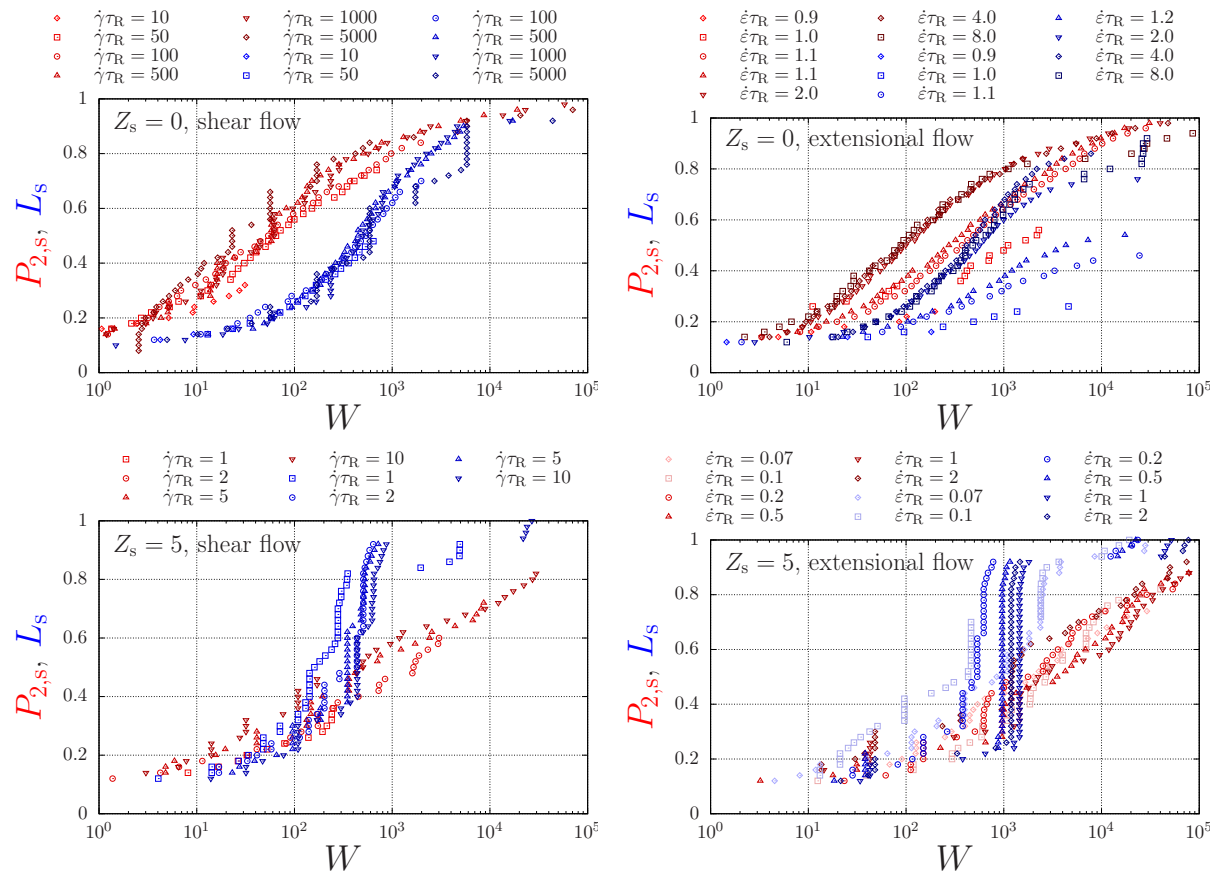


FIG. 11. Nematic order parameter,  $P_{2,s}$  and characteristic stretch ratio,  $L_s$ , against the specific work (see main text) for sticky (red) and non-sticky (blue) polymers in shear (left) and extensional (right) flow. The symbols are obtained from simulations with various strain rates for a chain with  $Z_s = 5$  with an elastically compliant network. All physical parameter values are given in Table I.

523 The top panels of this Figure give the nematic order parameter,  $P_{2,s}$ , and the measure  
 524 for stretch fluctuations,  $L_s$  against the critical specific work. For large values of the criti-  
 525 cal work, both measures converge, which suggests that both measures can interchangeably  
 526 used as predictors for flow-induced crystallisation for non-sticky chains. We notice that  
 527 the critical work in shear (left) and extensional flow (right) show similar trends well above  
 528 the stretch transition (the stretch transition of the bare chain is  $\dot{\epsilon}\tau_R = 1$ ). Just above  
 529 this transition the critical work required is relatively large. This implies a monotonically  
 530 decreasing critical work with an increasing strain rate, which is due to the suppression of  
 531 energy dissipation by recoiling of the chains (we discuss this in more detail in Fig. 12). This

This is the author's peer reviewed, accepted manuscript. However, the online version of record will be different from this version once it has been copyedited and typeset.

PLEASE CITE THIS ARTICLE AS DOI: 10.1122/8.0000411

532 is in contrast to the typical behaviour in experiments on non-associating polymers (e.g., the  
 533 flow-induced crystallisation of HDPE<sup>7</sup>), where the critical work *increases* with an increasing  
 534 strain rate. We argue this discrepancy occurs because we here consider unentangled rather  
 535 than entangled chains. Finally, the top panels of Fig. 11 confirm the expected behaviour  
 536 where the nematic order parameter (red) is typically larger than the stretching parameter  
 537 (blue): with an increasing specific work the chains first align and then stretch.

538 This behaviour is crucially altered for the sticky polymers, as shown in the bottom pan-  
 539 els of Fig. 11. We find that the alignment of the chains requires more critical work both  
 540 in shear (left) and extensional flow (right), which is due to the fact that the full alignment  
 541 of the chains requires the opening of intermolecular associations. On the other hand, the  
 542 stretching of chain segments can take place before global chain alignment. (Note that the  
 543 stretch transition is  $\dot{\epsilon}\tau_R \approx 0.1$  for this system, see Table I) The stretching parameter (blue)  
 544 follows a sharp sigmoidal dependence against the critical work, and rapidly outgrows the  
 545 alignment parameter (red) This is possible because the stretching parameter provides in-  
 546 formation about a fraction  $P_s = 1/500$  of chains in the tail of the distribution, while the  
 547 alignment parameter provides information about the mean properties. This supports out  
 548 hypothesis that flow-induced crystallisation may be achieved at a small critical specific work  
 549 by exploiting the stochastic nature of associating polymers.

550 Given either a  $L_s$  or  $P_{2,s}$  criterion for critical nucleation, we are interested how the strain  
 551 rate affects how much critical specific work,  $W$ , is needed, and at what timescale,  $t_s$  this  
 552 criterion is achieved. To investigate this, we focus on horizontal lines / cross sections of  
 553 Fig. 12 (i.e., at fixed values 0.6 and 0.8 of both  $L_s$  and  $P_{2,s}$ ). For the data points along these  
 554 lines we plot the critical work,  $W$ , and the timescale,  $t_s$ , in Fig. 12. The left panel shows  
 555 that the timescale scales as  $t_s \propto Wi^{-1}$ , as one may expect and discuss in more detail below.  
 556 Below the stretch transition this dependence becomes stronger: under these conditions many  
 557 chain stretches are attempted, but fail due to sticker opening and lead to energy dissipation  
 558 through chain retraction. This crossover between two regimes qualitatively agrees with that  
 559 found in Figure 2 of the work by Holland et al. on silk<sup>7</sup>; more dedicated research is needed  
 560 to investigate this observation.

561 The right panel of Fig. 12 shows the critical specific work needed to achieve a certain  
 562 degree of alignment,  $P_{2,s}$  (red), or of stretch fluctuations,  $L_s$  (blue), in shear (open symbols)  
 563 and extensional flow (closed symbols), against the sticky Weissenberg number. Evidently, a

This is the author's peer reviewed, accepted manuscript. However, the online version of record will be different from this version once it has been copyedited and typeset.

PLEASE CITE THIS ARTICLE AS DOI: 10.1122/8.0000411

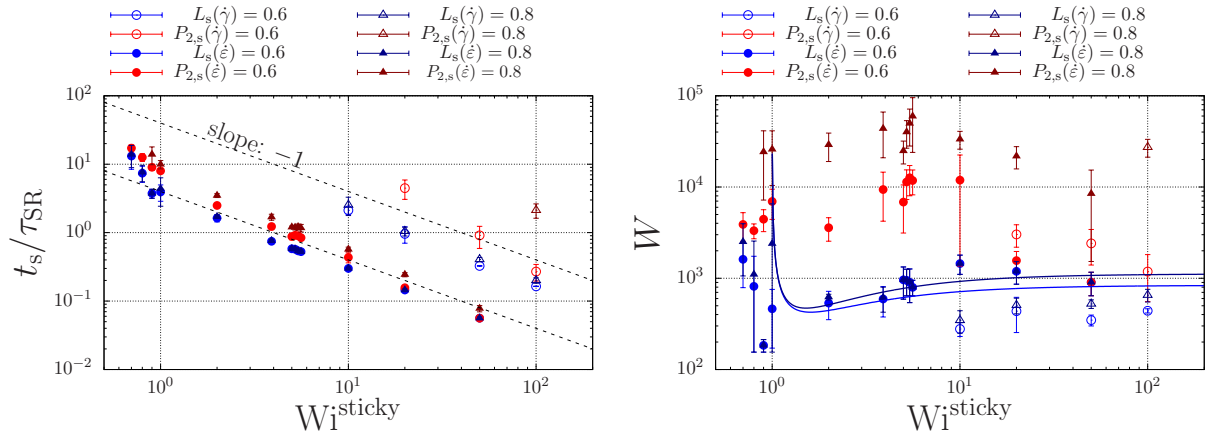


FIG. 12. The critical time (left) and the specific critical work (right) against the sticky Weissenberg number,  $Wi^{sticky} = \dot{\epsilon}\tau_{SR}, \dot{\gamma}\tau_{SR}$ , for various  $L_s$  and  $P_{2,s}$  criteria for the critical condition. The open symbols were calculated in shear and the closed ones in extensional flow. The values are obtained for a chain with  $Z_s = 5$  with an elastically compliant network. It is useful to interpret the strain rates in relation to the stretch transition for the sticky chains in extension at  $Wi^{sticky} = 1$ , where the ‘sticky’ Weissenberg number is  $Wi^{sticky} \approx 10Wi = 10\dot{\epsilon}\tau_R$ , with  $Wi$  the Weissenberg number of the non-sticky chain. This factor 10 is non-universal and depends on the number and lifetime of stickers, see Table I for all physical parameter values. The solid curves are given by Eq. (40) for  $L_s = 0.6$  and for  $L_s = 0.8$ .

564 high degree of overall alignment / nematic order requires much larger specific work than a  
 565 small fraction of large stretch fluctuations does, as discussed in Fig. 11. Having in mind our  
 566 overarching proposition that crystallisation may occur in response to stretch fluctuations,  
 567 we now focus on the measure for  $L_s$ . We remark that for the system we studied, the  
 568 stretch transition in the absence of stickers takes is located at  $Wi^{sticky} = \dot{\epsilon}\tau_{SR} \approx 10$  (because  
 569  $\tau_{SR} \approx 10\tau_R$ , see Table I). For smaller strain rates,  $Wi^{sticky} < 10$ , we find there is a minimum in  
 570 the specific critical work near the stretch transition  $Wi^{sticky} \approx 1$ . Indeed, while large stretches  
 571 are achieved just below the stretch transition  $Wi^{sticky} < 1$  due to long power-law tails in the  
 572 stretch distribution<sup>10</sup>, many of attempt fluctuations are needed before the required stretch  
 573 value is achieved. Due to the energy dissipation of such unsuccessful attempts, the specific  
 574 critical work increases for decreasing strain rates. Above the minimum, the specific work  
 575 increases and eventually reaches a plateau.

576 We explain the increase of the critical specific work with an increasing strain rate in terms

577 of the two-state model that we introduced in the Theory section. We argue that the stress  
578 is dominated by the contributions of stretched chains in the closed state,

$$\sigma_{xx}(t) = c \int P_0(\lambda, t) \lambda(t)^2 d\lambda, \quad (37)$$

579 with  $c$  a constant, assuming that the open chains are in a relaxed state. Here,  $P_0(\lambda, t)$  is  
580 the stretch distribution of the closed chains, of which we will discuss the dynamics below.  
581 We will then calculate the critical specific work as  $W = \int_0^{t_s} \sigma_{xx} \dot{\epsilon} dt$ . To calculate  $W$ , we first  
582 will determine  $t_s$  using the criterion

$$\int_{L_s \lambda_{\max, i}}^{\lambda_{\max, i}} P_0(\lambda, t_s) d\lambda \geq P_s, \quad (38)$$

583 which, as before, implies a minimum concentration of chains with a stretch ratio of at least  
584  $\lambda_s = L_s \lambda_{\max, i}$ . Secondly, we will need an expression for the time evolution of the probability  
585 density  $P_0$ .

586 To obtain  $P_0$ , we will assume that all chains that have (temporarily) opened are suffi-  
587 ciently relaxed compared to the most stretched chains to have a negligible contribution to  
588 the overall stress  $\sigma_{xx}$ . Therefore, we will only take into account the loss of strongly stretched  
589 chains by opening rate  $k_{\text{open}}$ , and ignore the contribution of closing events by rate  $k_{\text{close}}$ . We  
590 will further use the initial condition  $P(\lambda, 0) = \delta(1 - \lambda)$ , with  $\delta(\cdot)$  the Dirac delta distribution  
591 to represent a narrow stretch distribution at time  $t = 0$ . The dynamical equation in Eq. (21)  
592 then predicts that the Dirac delta distribution in time shifts to high stretch values along the  
593  $\lambda$  axis, as

$$P_0(\lambda, t) = \delta(\ln \lambda - \dot{\epsilon} t) \lambda^{-(1+1/(\dot{\epsilon} \tau_s))}, \quad (39)$$

594 with an amplitude that decreases in time due to sticker opening (we present the derivation  
595 in the first two paragraphs of Appendix VB).

596 Eq. (39) shows that the critical stretch and the critical time are related by  $t_s = \ln \lambda_s / \dot{\epsilon}$ ,  
597 which is in agreement with our simulated results displayed in Fig. 11. We insert this equation  
598 into the expression for the critical specific work,  $W = \int_0^{t_s} \sigma_{xx} \dot{\epsilon} dt$ , and find

$$W(\dot{\epsilon}) = c \left(1 - \frac{1}{\dot{\epsilon} \tau_s}\right)^{-1} \exp \left[ \left(1 - \frac{1}{\dot{\epsilon} \tau_s}\right) \ln \lambda_s - 1 \right], \quad \text{for } \dot{\epsilon} > \dot{\epsilon}_{\min}, \quad (40)$$

599 where  $\dot{\epsilon}_{\min}$  is the minimum strain rate for which the criterion in Eq. (38) is obeyed. This  
600 function is plotted in Fig. 12(b). It diverges at  $\dot{\epsilon} \tau_s = 1$  (this divergence is not followed

601 by the simulation data, because stochastic closing events that generate new bound chain  
602 segments), reaches a minimum, and then monotonically increases towards a plateau value.  
603 Physically, this plateau value represents the case where the entire distribution of chains is  
604 stretched to reach the critical stretch value  $\lambda_s$ . In this case, the concentration of stretched  
605 segments far exceeds the critical concentration, and more energy has been put into the  
606 system than needed. By decreasing the strain rate, an increasing number of stickers are able  
607 to open and the stress is relaxed, in turn decreasing the critical specific work to achieve the  
608 critical condition in Eq. (38). This supports our proposition that the stochastic nature of the  
609 binding and unbinding of associations enables to molecularly engineer associating polymers  
610 to undergo flow-induced crystallisation at low energetic costs. In particular, we have shown,  
611 using simulations and an approximate theory in Eq. (40) that there is an *optimum* strain  
612 rate at which the critical work for critical stretch is minimised

#### 613 IV. DISCUSSION AND CONCLUSIONS

614 This work has shown that the transient evolution of the chain-stretch distribution of  
615 associating ‘sticky’ polymers in shear, and especially extensional, flow possesses an extremely  
616 rich structure. The theoretical and numerical investigations reported here were driven by  
617 the observation that the silk protein (i) undergoes efficient, chemically tunable, flow-induced  
618 crystallisation and (ii) can be modelled as an associating/sticky polymer. Our findings have  
619 implications for the interpretation of silk-spinning data, as well as to the development of  
620 novel associating polymers and the computational modelling tools (we introduced a ‘sticky’  
621 sliplink model, and an analytical two-state master equation which may be transferable to  
622 also address the peculiar dynamics of ring polymer in flow<sup>43–45</sup>).

623 Regarding silk rheology, we have theoretically confirmed our hypothesis that the stickers  
624 between chains may reduce the critical specific work to induce flow-induced crystallisation  
625 (FIC) under reasonable assumptions for critical crystallisation criteria. In our approach, we  
626 have adopted the view that FIC may commence when a sufficient concentration of chains is  
627 aligned at the level of the Kuhn segments. However, in contrast to the ensemble-averaged  
628 approach where the Kuhn segmental nematic order parameter is measured as a predictor for  
629 FIC, we have assumed that a critical concentration of strongly stretched chain segments *in*  
630 *the tail of the distribution* is a sufficient condition for crystallisation. Indeed, by comparing a

This is the author's peer reviewed, accepted manuscript. However, the online version of record will be different from this version once it has been copyedited and typeset.

PLEASE CITE THIS ARTICLE AS DOI: 10.1122/1.5000041

631 measure for the stretch fluctuations to the (ensemble-average) nematic order parameter, we  
632 have found that the stickers hamper initial chain alignment (chain alignment is slowed down  
633 by the need for stickers to dissociate), while segmental stretch is facilitated by the closed  
634 stickers. Importantly, our analysis revealed that the incorporation of stickers enables a  
635 significant reduction in the input of specific work needed to achieve large stretch fluctuations,  
636 and consequently, may reduce the energy requirements for FIC.

637 Focussing on our finding that chain alignment at low, non-stretching, flow rates requires  
638 less specific work in the absence of stickers (and presumably for low sticker lifetimes) than  
639 with stickers, while the stretching of the chains at high rates is helped by long sticker life-  
640 times, we speculate that control over both the structural aspects of the final material and  
641 over the specific work needed is possible through time- or position-dependent sticker life-  
642 times. We argue this can be achieved through external chemical control. Indeed, during its  
643 larval life cycle, the silkworm stably stores its silk solution at a high viscosity, but just prior  
644 to silk spinning it lowers the viscosity through an increase of the potassium concentration  
645 through a decreasing lifetime of calcium bridges (stickers)<sup>8,9</sup>. This, as we can now interpret  
646 as a mechanism to ease chain alignment in flow. Intriguingly, downstream the spinning duct  
647 the acidity increases<sup>34</sup>, which we expect to increase the stability and hence the lifetime of  
648 the calcium bridges, and hence enhance local chain stretching, see Fig. 1, which may in turn  
649 disrupts the solvation layer of the protein and induce efficient crystallisation<sup>7,13,15-18</sup>.

650 While this seems a compelling mechanism for efficient flow-induced crystallisation, it is  
651 not yet clear how this process may be optimised. The experimental accessibility of these  
652 and other questions has come in reach owing to recent advances in controlling the content  
653 of metal cations in silk feedstock<sup>70</sup>. In the case of *Bombyx mori* silk, we identified a regular  
654 spacing of the negative charges along the backbone of the chain, with strands of approxi-  
655 mately 500 uncharged amino acids between; the length of these sticker strands is of the order  
656 of the entanglement molecular weight<sup>9</sup>. The regularity of the spacing and the coincidental  
657 similarity between the number of stickers and entanglements suggests some degree of evo-  
658 lutionary optimisation. The functionality of ordered- versus random co-polymers is of high  
659 importance from a synthetic polymer chemistry point of view, and needs to be addressed  
660 using simulations that include both associations and entanglements.

661 We conclude that our modelling approach leaves us well prepared to investigate the ways  
662 in which the evolution of silk-producing organisms may have exploited the potential optimal

663 strategies for efficient fibre processing. The next piece of physics to add to this account of  
 664 the rheology of polymers with temporary associations, not only for modelling silk proteins  
 665 but also general associating polymers, concerns the interaction between entanglements and  
 666 associations in strong flow. We anticipate that this will further enrich the ongoing debate  
 667 in polymer physics on the physics of entanglement generation and destruction (i.e., ‘en-  
 668 tanglement stripping’) in non-linear rheo-physics, as well as continue the account of how  
 669 silk-forming organisms point to novel rheo-physics of flow-induced phase-transformations.

## 670 V. APPENDIX

### 671 A. Algorithm

672 Because of the large distribution of chain stretch in the conditions we are interested in,  
 673 there is also a large distribution of opening rates; in our previous work we used small time  
 674 steps in which the chain conformation was updated, and each closed pair had a sufficiently  
 675 small opening probability. Here, we significantly improve this algorithm by enabling much  
 676 larger time steps between conformational updates, and during which the stickers may open  
 677 and close many times, see Fig. 3.

678 In our algorithm, we update the *chain conformation* using the Brownian dynamics equa-  
 679 tion from the previous section using a time span  $\Delta t$ . Depending on the opening and closing  
 680 rates, during this time span,  $\Delta t_1 \equiv \Delta t$ , the *sticker configuration* may be updated many times  
 681 or not at all according to a kinetic Monte Carlo (kMC) scheme<sup>64-66</sup>. In every kMC step, the  
 682 rate at which any opening or closing event may occur is calculated as  $W_T = W_a + W_d$ , with

$$W_a = k_a N_{\text{open}}(N_{\text{open}} - 1)/2, \quad (41)$$

683 the sum of closing rates and

$$W_d = \sum_{q=1}^{N_{\text{closed}}/2} k_{d,q}, \quad (42)$$

684 the sum of dissociation rates, where  $k_{d,q}$  differs for the different sticker pairs due to dispersity  
 685 in chain tension. In these expressions,  $N_{\text{open}}$  and  $N_{\text{closed}}$  are the number of open and closed  
 686 stickers, respectively;  $N_{\text{open}}(N_{\text{open}} - 1)/2$  is the total number of possible associations, and  
 687 the index  $q$  sums over all  $N_{\text{closed}}/2$  *pairs* of closed stickers. Using this sum of rates, the time

688  $\Delta t_2$  at which the first opening or closing event occurs is

$$\Delta t_2 = -\frac{1}{W_T} \ln(u), \quad (43)$$

689 with  $u \in (0, 1]$  a uniform random number (our code uses random numbers using the open-  
 690 source SFMT library<sup>71</sup>). If  $\Delta t_2$  exceeds the time span  $\Delta t_1$ , no opening or closing events  
 691 occurs. However, if  $\Delta t_2 < \Delta t_1$  then a second random number  $\in [0, 1]$  is drawn, and a  
 692 closing event is selected with probability  $k_a/W_T$ , and a dissociation event  $q$  is selected with  
 693 probability  $k_{d,q}/W_T$ . After updating the configurations of the stickers, the time span is  
 694 updated to  $\Delta t_1 = \Delta t_1 + \Delta t_2$ . The kMC scheme is terminated when  $\Delta t_2 > \Delta t_1$ , following  
 695 which the chain conformation is updated.

696 While in the linear rheological conditions we solve the dynamics using a fixed time step, in  
 697 strong flow we implemented an adaptive time step to handle the large and fast fluctuations  
 698 in stretch that emerge in some parameter regimes of the system. In every iteration  $n$ , the  
 699 time step for the next iteration is updated as

$$\Delta t^{n+1} = \Delta t^n \left( \min_i \frac{\text{tolerance}}{\text{error}} \right)^{0.25}, \quad (44)$$

700 where an error and tolerance are calculated for the change of each end-to-end vector  $\mathbf{Q}_i$ .  
 701 We defined the error value for each change in  $Q_i$  as  $\text{error} = |\Delta Q_i^n|/Q_{\max}$ , with  $Q_{\max}$  set by  
 702  $\lambda_{\max}$ . For the tolerance value we use scalar values  $\text{tol}_-$  and  $\text{tol}_+$  depending on whether  $|Q_i^n|$   
 703 is smaller or larger than a certain cutoff set by  $\lambda_{\text{cutoff}} < \lambda_{\max}$ . Above the cutoff, we avoid  
 704 numerical instabilities due to the singularity at  $\lambda_{\max}$  by using

$$k_s(\lambda > \lambda_{\text{cutoff}}) = k_s(\lambda_{\text{cutoff}}) \times \left( \frac{\lambda}{\lambda_{\text{cutoff}}} \right)^\alpha. \quad (45)$$

705 For continuity of the derivative,  $\alpha = 4c^2/(3 - 4c^2 + c^4)$ , with  $c = \lambda_{\text{cutoff}}/\lambda_{\max}$ ; for a cutoff  
 706  $\lambda_{\text{cutoff}} = 0.9\lambda_{\max}$  even this smooth potential is steep ( $\alpha \approx 8$ ), and in practice we use a softer  
 707 potential ( $\alpha = 4$ ).

## 708 B. Asymptotic limits of the two-state model

The two-state master equation in Eqs. (21-22) has analytical solutions for early times where advection dominates over the sticker dynamics, and for late times where the sticker dynamics is fast compared to the rate by which the deep tail of the stretch distribution

fills up. We obtain these analytical solutions in both cases using the Laplace transform of Eqs. (21-22) in the limit of large stretches  $\lambda > \lambda_* \gg 1$ , which is

$$\frac{\partial \tilde{P}_0}{\partial y} = -(k_{\text{open}} + \dot{\epsilon} + s)\tilde{P}_0 + k_{\text{close}}\tilde{P}_1 + P_0(0, y)/s, \quad (46)$$

$$\frac{\partial \tilde{P}_1}{\partial y} = +k_{\text{open}}\tilde{P}_0 - (k_{\text{close}} + \dot{\epsilon} + s - \tau_{\text{R}}^{-1})\tilde{P}_1 + P_1(0, y)/s, \quad (47)$$

709 where  $\tilde{P}_i(s, y) \equiv \mathcal{L}\{P_i(t, y)\}$  is the Laplace transform of  $P_i$  for  $i = 0, 1$  (hence, we have used  
710 the standard Laplace transform of the time derivative  $\mathcal{L}\{\partial P_i/\partial t\} = s\tilde{P}_i(s, y) - P_i(0, y)$ ). We  
711 will obtain the early- and late-stage solutions by using different initial conditions  $P_i(0, y)$  at  
712  $t = 0$  and boundary conditions that we will discuss below.

713 Focussing first on the early-stage limit, we consider a narrow distribution  $P(\lambda, 0) =$   
714  $\delta(1 - \lambda_*)$  of chain segments between closed stickers at time  $t = 0$ , with  $\delta(\cdot)$  the Dirac  
715 delta distribution. For early times, these segments stretch exponentially with time until the  
716 stickers open. To inspect how these segments evolve, we insert the initial conditions into  
717 Eq. (46), which gives

$$\frac{\partial \tilde{P}_0}{\partial y}(\lambda, s) = -(k_{\text{open}} + \dot{\epsilon} + s)\tilde{P}_0(\lambda, s) + c\delta(1 - \lambda), \quad (48)$$

718 with  $\tilde{P}_0(\lambda, s)$  the Laplace transform of  $P_0(\lambda, s)$ . The solution is of the standard form  $\tilde{P}_0 \propto$   
719  $\exp(-s\tau)$ , which after inverse Laplace transform gives Eq. (39) in the main text.

To solve Eqs. (21-22) in the long-time limit, we make the useful approximation that at an intermediate time  $t = t_*$  the distribution is at steady state for small stretches  $\lambda \leq \lambda_*$ , while the large-stretch tail of the distribution is unoccupied. Hence, at  $t = t_*$  the distribution is given by

$$P_0(0, y) = \frac{c'}{c}P_0^{\text{eq}}\Theta(-y + y_*) \quad (49)$$

$$P_1(0, y) = \frac{c'}{c}P_1^{\text{eq}}\Theta(-y + y_*), \quad (50)$$

720 where  $y_* \equiv \ln \lambda_*$  and where  $\Theta$  is the Heaviside step function. The prefactor

$$c' = \left(1 + c\frac{1}{1 + \nu}e^{(1+\nu)y_*}\right)^{-1} > 1, \quad (51)$$

721 normalises the distribution. We now set  $\lambda_*$  to a large value, so  $c' \approx c$ , and at late times  
722  $t > t_*$  the filling of the tail of the distribution (for  $\lambda > \lambda_*$ ) occurs with a negligible effect on  
723 the distribution at small stretches.

of which the solution is of the form

$$\tilde{P}_0(s, \lambda) = c_0^+(s)\lambda^{\nu_+(s)} + c_0^-(s)\lambda^{\nu_-(s)} \quad (52)$$

$$\tilde{P}_1(s, \lambda) = c_1^+(s)\lambda^{\nu_+(s)} + c_1^-(s)\lambda^{\nu_-(s)}, \quad (53)$$

with  $\nu_-(s)$  and  $\nu_+(s)$  the eigenvalues given by

$$\nu_{\pm} = \frac{1}{2\dot{\epsilon}(1 - \dot{\epsilon}\tau_R)} \left( (2\dot{\epsilon} + k_{\text{open}})(1 - \dot{\epsilon}\tau_R) - \dot{\epsilon}\tau_R k_{\text{close}} + s(1 - 2\dot{\epsilon}\tau_R) \right. \\ \left. \pm \sqrt{(s + k_{\text{open}}(1 - \dot{\epsilon}\tau_R))^2 + 2\dot{\epsilon}\tau_R(s - (1 - \dot{\epsilon}\tau_R)k_{\text{open}})k_{\text{close}} + (\dot{\epsilon}\tau_R k_{\text{close}})^2} \right), \quad (54)$$

724 and where the coefficients,  $c_i^{\pm}$ , follow from the boundary condition at  $y = y_*$ .

725 At late times, i.e., for small  $s$ , we have  $\nu_-(s) \approx \nu_{\text{eq}} - (s/\dot{\epsilon})\nu' + (1/2)(s/\dot{\epsilon})^2\nu''$ , where  $\nu_{\text{eq}}$   
726 is given by Eq. (25), and where

$$\nu' \equiv \left. \frac{d\nu}{d(s/\dot{\epsilon})} \right|_{s=0} = \left( 1 - \frac{1}{1 - \text{Wi}} + \frac{1}{1 - \text{Wi}^{\text{sticky}}} \right), \quad (55)$$

727 and

$$\nu'' \equiv 2p\text{Wi} \frac{\text{Wi}^{\text{sticky}}}{(1 - \text{Wi}^{\text{sticky}})^3}, \quad (56)$$

728 are both positive, provided that the sticky Weissenberg number is sufficiently small,  
729  $\text{Wi}^{\text{sticky}} \equiv \text{Wi}/(1 - p) < 1^{10}$ , where  $\text{Wi} = \dot{\epsilon}\tau_R$  is the Weissenberg number of the chain  
730 without stickers.

From the boundary condition, we find that the coefficients must be of the form  $c_i^{\pm} \propto 1/s$ .  
As the ‘+’ solution leads to a non-normalisable solution, however,  $c_i^+ = 0$ , and the solution  
is

$$\tilde{P}_0(s, \lambda) = \frac{c}{s} (\lambda/\lambda_*)^{\nu_-(s/\dot{\epsilon}) - \frac{1}{2}(s/\dot{\epsilon})^2\nu'' + \mathcal{O}(s^3)}, \quad (57)$$

$$\tilde{P}_1(s, \lambda) = \frac{k_{\text{close}}}{k_{\text{open}}} \frac{\dot{\epsilon}}{(\dot{\epsilon} - \tau_R^{-1})} \tilde{P}_0(s, \lambda). \quad (58)$$

Finally, after taking the inverse Laplace transform, we have

$$P_0(t, \lambda) = c \left( \frac{\lambda}{\lambda_*(0)} \right)^{\nu_{\text{eq}}} \Theta(\nu' \ln \lambda/\lambda_* - \dot{\epsilon}t) \quad (59)$$

$$P_1(t, \lambda) = \frac{k_{\text{close}}}{k_{\text{open}}} \frac{\dot{\epsilon}}{(\dot{\epsilon} - \tau_R^{-1})} P_0(t, \lambda). \quad (60)$$

731 Hence, the exponentially extending front of the distribution is located at the stretch ratio

$$\lambda_*(t) = \lambda_*(0) \exp \left[ \left( 1 - \frac{1}{1 - \text{Wi}} + \frac{1}{1 - \text{Wi}^{\text{sticky}}} \right)^{-1} \dot{\epsilon}(t - t_*) \right]. \quad (61)$$

732 We have checked the validity of our interpretation of a narrow moving-front by also  
733 calculating the width of this front. To do this, we consider the relaxation function  $f(t) =$   
734  $P(y, t)/P_{\text{eq}}(y)$  with again  $y = \ln \lambda$ , and  $P$  and  $P_{\text{eq}}$  the transient and steady-state stretch  
735 distributions, respectively. A narrow front that reaches  $y$  at time  $\tau$  and reaches a steady  
736 state at time  $\tau + \Delta$  may be approximated by

$$f(t) = \begin{cases} 0, & \text{for } t < \tau \\ (t - \tau)/\Delta, & \text{for } \tau \leq t < \tau + \Delta \\ 1, & \text{for } t \geq \tau + \Delta. \end{cases} \quad (62)$$

737 The Laplace transform of this function is

$$\mathcal{L}\{f\} = \frac{1}{s^2 \Delta} e^{-s\tau} (1 - e^{-s\Delta}). \quad (63)$$

738 We compare this result to the solution of the two-state model in Eq. (54) through a second-  
739 order Taylor expansion of the exponential terms

$$\mathcal{L}\{f\} = \frac{1}{s} \left( 1 - \underbrace{\left( \tau + \frac{1}{2} \Delta \right) s}_{(\nu'/\dot{\epsilon}) \ln y} + \frac{1}{2} \underbrace{\left( \tau^2 + \frac{1}{3} \Delta^2 + \Delta \tau \right) s^2}_{(\nu''/\dot{\epsilon}^2) \ln y} \right). \quad (64)$$

740 From the linear term, we find  $\tau + \Delta/2 = (\nu'/\dot{\epsilon}) \ln y$  (as expected from Eq. (29)). After  
741 substitution into the second term and elimination of this variable, we find the width of the  
742 front to be

$$\Delta = \sqrt{12} \sqrt{(\nu''/\dot{\epsilon}) \ln y - (\nu'/\dot{\epsilon})^2 \ln y}. \quad (65)$$

743 The relative width, compared to the location of the front  $(\tau + \Delta/2)$ , is

$$\Delta_{\text{rel}} \equiv \frac{\Delta}{\tau + \Delta/2} = \sqrt{12} \sqrt{\frac{\nu''}{(\nu')^2} - 1} \quad (66)$$

744 The relative width calculated in the time-domain also represents the relative width of the  
745 (logarithmic) stretch distribution:

$$\Delta_{\text{rel}} \equiv \frac{y(\tau + \Delta) - y(\tau)}{y(\tau + \Delta/2)}. \quad (67)$$

746 Upon approaching the strain rate where the mean stretch diverges, i.e., at  $Wi^{\text{sticky}} = 1$ ,  
 747 the relative width of the front diverges as  $\Delta_{\text{rel}} \approx \sqrt{24pWiWi^{\text{sticky}}/(1 - Wi^{\text{sticky}})}$ . In this  
 748 equation, the bare Weissenberg number is  $Wi = Wi^{\text{sticky}}(1 - p)\tau_R/\tau_s$ . Hence, if the sticker  
 749 lifetime is  $\tau_s = 10\tau_R$  and the fraction of closed stickers is  $p = 0.9$  (as in our simulations),  
 750 then significant broadening of the front only happens very close to the stretch transition:  
 751  $Wi^{\text{sticky}} > 0.99$ . This verifies that our approximation of a narrow front is indeed accurate.

### 752 C. Power-law regression

753 To determine the sticky Rouse diffusivity,  $D_{\text{SR}}$ , from the mean-square displacement of  
 754 the centre of mass

$$\ln \text{MSD} = \ln(6D_{\text{SR}}) + \ln t \quad (68)$$

755 as a function of time  $t$ , and the stretch exponent,  $\nu$ , from the probability distribution

$$\ln P = c + \nu \ln \lambda \quad (69)$$

756 as a function of the stretch ratio,  $\lambda$ , we write both equations in the form

$$y = a + bx \quad (70)$$

757 and perform common linear regression. However, because both power-laws represent asymp-  
 758 totic behaviour for large  $x$ , there is also a cutoff value,  $x_{\text{cutoff}}$ , above which they apply. We  
 759 determine the cutoff by minimising

$$\chi^2(a, b, i_0) \equiv \frac{1}{N_{\text{data}} + 1 - i_0 - N_{\text{par}}} \sum_{i=i_0}^{N_{\text{data}}} \frac{(y_i^{\text{data}} - y_i^{\text{fit}}(a, b))^2}{\sigma_i^2}, \quad (71)$$

760 with respect to  $a$ ,  $b$  and  $i_0$  (note that  $x_{i_0} = x_{\text{cutoff}}$ );  $\sigma_i$  is the uncertainty on the simulated  $y$   
 761 data. Here, we set  $b = 1$  fixed and the number of free parameters  $N_{\text{par}} = 1$  for extracting the  
 762 sticky Rouse diffusivity from the MSD data. To determine the stretch exponent ( $\nu$ ) from  
 763 the stretch distributions we use the same approach, but leave  $b$  as a free fitting parameter  
 764 and set  $N_{\text{par}} = 2$ .

### 765 ACKNOWLEDGMENTS

766 This research was funded by the Engineering and Physical Sciences Research Council  
 767 [grant number EPSRC (EP/N031431/1)]. C.S. is grateful for the computational support

This is the author's peer reviewed, accepted manuscript. However, the online version of record will be different from this version once it has been copyedited and typeset.

PLEASE CITE THIS ARTICLE AS DOI: 10.1122/1.5111111

768 from the University of York high-performance computing service (the Viking Cluster), and  
769 thanks Daniel J. Read for his suggestion to pair closed stickers of different chains. C.S. and  
770 T.C.B.M. thank Pete Laity and Chris Holland for useful discussions on the mechanism of  
771 silk self-assembly.

## 772 REFERENCES

- 773 <sup>1</sup>R. S. Graham and P. D. Olmsted, “Coarse-grained simulations of flow-induced nucleation  
774 in semicrystalline polymers,” *Phys. Rev. Lett.* **103**, 115702 (2009).
- 775 <sup>2</sup>E. M. Troise, H. J. M. Caelers, and G. W. M. Peters, “Full characterization of multiphase,  
776 multimorphological kinetics in flow-induced crystallization of ipp at elevated pressure,”  
777 *Macromolecules* **50**, 3868–3882 (2017).
- 778 <sup>3</sup>D. A. Nicholson and G. C. Rutledge, “An assessment of models for flow-enhanced nucle-  
779 ation in an n-alkane melt by molecular simulation,” *J. Rheol.* **63**, 465–475 (2019).
- 780 <sup>4</sup>S. Moghadamand, I. S. Dalal, and R. G. Larson, “Unraveling dynamics of entangled  
781 polymers in strong extensional flows,” *Macromolecules* **52**, 1296–1307 (2019).
- 782 <sup>5</sup>R. S. Graham, “Understanding flow-induced crystallization in polymers: A perspective on  
783 the role of molecular simulations,” *J. Rheol.* **63**, 203–214 (2019).
- 784 <sup>6</sup>D. J. Read, C. McIlroy, C. Das, O. G. Harlen, and R. S. Graham, “Polystrand model of  
785 flow-induced nucleation in polymers,” *Phys. Rev. Lett.* **124**, 147802 (2020).
- 786 <sup>7</sup>C. Holland, F. Vollrath, A. J. Ryan, and O. O. Mykhaylyk, “Silk and synthetic polymers:  
787 reconciling 100 degrees of separation,” *Adv. Mater.* **24**, 105–109 (2012).
- 788 <sup>8</sup>P. R. Laity, E. Baldwin, and C. Holland, “Changes in silk feedstock rheology during  
789 cocoon construction: the role of calcium and potassium ions,” *Macromol. Biosci.* **0**, 1800188  
790 (2018).
- 791 <sup>9</sup>C. Schaefer, P. R. Laity, C. Holland, and T. C. B. McLeish, “Silk protein solution: A  
792 natural example of sticky reptation,” *Macromolecules* **53**, 2669–2676 (2020).
- 793 <sup>10</sup>C. Schaefer and T. C. B. McLeish, “Power-law stretching of associating polymers in steady-  
794 state extensional flow,” *Phys. Rev. Lett.* **126**, 057801 (2021).
- 795 <sup>11</sup>C. Schaefer, P. R. Laity, C. Holland, and T. C. B. McLeish, “Stretching of bombyx mori  
796 silk protein in flow,” *Molecules* **26**, 1663 (2021).

This is the author's peer reviewed, accepted manuscript. However, the online version of record will be different from this version once it has been copyedited and typeset.

PLEASE CITE THIS ARTICLE AS DOI: 10.1122/1.5111111

- 797 <sup>12</sup>T. Asakura, “Structure of silk i (bombyx mori silk fibroin before spinning)-type ii -turn,  
798 not -helix-,” *Molecules* **26**, 3706 (2021).
- 799 <sup>13</sup>G. J. Dunderdale, S. J. Davidson, A. J. Ryan, and O. O. Mykhaylyk, “Flow-induced  
800 crystallisation of polymers from aqueous solution,” *Nat. Comm.* **11**, 3372 (2020).
- 801 <sup>14</sup>P. R. Laity and C. Holland, “Seeking solvation: Exploring the role of protein hydration in  
802 silk gelation,” *Molecules* **25**, 551 (2020).
- 803 <sup>15</sup>S. Donets and J.-U. Sommer, “Molecular dynamics simulations of strain-induced phase  
804 transition of poly(ethylene oxide) in water,” *J. Phys. Chem. B* **122**, 392 (2018).
- 805 <sup>16</sup>S. Donets, O. Guskova, and J.-U. Sommer, “Flow-induced formation of thin peo fibres in  
806 water and their stability after the strain release,” *J. Phys. Chem. B* **124**, 9224 (2020).
- 807 <sup>17</sup>S. Donets, O. Guskova, and J.-U. Sommer, “Searching for aquamelt behavior among  
808 silklike biomimetics during fibrillation under flow,” *J. Phys. Chem. B* **125**, 3238 (2021).
- 809 <sup>18</sup>W. D. Mkandawire and S. T. Milner, “Simulated osmotic equation of state for  
810 poly(ethylene oxide)solutions predicts tension-induced phase separation,” *Macromolecules*  
811 **54**, 3613 (2021).
- 812 <sup>19</sup>L. Leibler, M. Rubinstein, and R. H. Colby, “Dynamics of reversible networks,” *Macro-*  
813 *molecules* **24**, 4701–4707 (1991).
- 814 <sup>20</sup>R. H. Colby, X. Zheng, M. H. Rafailovich, J. Sokolov, D. G. Peiffer, S. A. Schwarz,  
815 Y. Strzhemechny, and D. Nguyen, “Dynamics of lightly sulfonated polystyrene ionomers,”  
816 *Phys. Rev. Lett.* **81**, 3876–3879 (1998).
- 817 <sup>21</sup>S. Hackelbusch, T. Rossow, P. van Assenbergh, and S. Seiffert, “Chain dynamics in  
818 supramolecular polymer networks,” *Macromolecules* **46**, 6273–6286 (2013).
- 819 <sup>22</sup>Q. Chen, Z. Zhang, and R. H. Colby, “Viscoelasticity of entangled random polystyrene  
820 ionomers,” *J. Rheol.* **60**, 1031–1040 (2016).
- 821 <sup>23</sup>T. Tomkovic and S. G. Hatzikiriakos, “Nonlinear rheology of poly(ethylene-co-methacrylic  
822 acid) ionomers,” *J. Rheol.* **62**, 1319–1329 (2018).
- 823 <sup>24</sup>Z. Zhang, Q. Chen, and R. H. Colby, “Dynamics of associative polymers,” *Soft Matter*  
824 **14**, 2961–2977 (2018).
- 825 <sup>25</sup>Z. R. Hinton, A. Shabbir, and N. J. Alvarez, “Dynamics of supramolecular self-healing  
826 recovery in extension,” *Macromolecules* **52**, 2231–2242 (2019).
- 827 <sup>26</sup>M. Golkaram and K. Loos, “A critical approach to polymer dynamics in supramolecular  
828 polymers,” *Macromolecules* **52**, 9427–9444 (2019).

This is the author's peer reviewed, accepted manuscript. However, the online version of record will be different from this version once it has been copyedited and typeset.

PLEASE CITE THIS ARTICLE AS DOI: 10.1122/1.511111

829 <sup>27</sup>M. Zuliki, S. Zhang, K. Nyamajaro, T. Tomkovic, and S. G. Hatzikiriakos, “Rheology of  
830 sodium and zinc ionomers: Effects of neutralization and valency,” *Phys. Fluids* **32**, 023104  
831 (2020).

832 <sup>28</sup>S. Liu, X. Cao, C. Huang, R. A. Weiss, Z. Zhang, and Q. Chen, “Brittle-to-ductile  
833 transition of sulfonated polystyrene ionomers,” *ACS. Macro. Lett.* **10**, 503–509 (2021).

834 <sup>29</sup>T. Witten, “Associating polymers and shear thickening,” *J. Phys. France* **49**, 1055–1063  
835 (1988).

836 <sup>30</sup>H.-J. Jin and D. L. Kaplan, “Mechanism of silk processing in insects and spiders,” *Nature*  
837 **424**, 1057–1061 (2003).

838 <sup>31</sup>F. Tanaka, R. Takeda, and K. Tsurusaki, “Critical shear rate for gelation in aqueous  
839 solutions of associating polymers under shear flows,” *J. Phys. Soc. Jpn.* **87**, 074801 (2018).

840 <sup>32</sup>Y. S  r  ro, V. Jacobsen, and J.-F. Berret, “Evidence of nonlinear chain stretching in the  
841 rheology of transient networks,” *Macromolecules* **33**, 1841–1847 (2000).

842 <sup>33</sup>A. Tripathi, K. C. Tam, and G. H. McKinley, “Rheology and dynamics of associative  
843 polymers in shear and extension: Theory and experiments,” *Macromolecules* **39**, 1981–  
844 1999 (2006).

845 <sup>34</sup>A. Koepfel, N. Stehling, C. Rodenburg, and C. Holland, “Spinning beta silks requires  
846 both pH activation and extensional stress,” *Adv. Func. Mater.* **31**, 2103295 (2021).

847 <sup>35</sup>H. Janeschitz-Kriegl, “How to understand nucleation in crystallizing polymer melts under  
848 real processing conditions,” *Colloid. Polym. Sci.* **281**, 1157–1171 (2003).

849 <sup>36</sup>O. O. Mykhaylyk, P. Chambon, R. S. Graham, J. Patrick, A. Fairclough, P. D. Olm-  
850 sted, and A. J. Ryan, “The specific work of flow as a criterion for orientation in polymer  
851 crystallization,” *Macromolecules* **41**, 1901–1904 (2008).

852 <sup>37</sup>J. Seo, A. M. Gohn, R. P. Schaake, D. Parisi, A. M. Rhoades, and R. H. Colby, “Shear  
853 flow-induced crystallization of poly(ether ether ketone),” *Macromolecules* **3472–3481**, 53  
854 (2020).

855 <sup>38</sup>A. E. Likhtman and T. C. B. McLeish, “Quantitative theory for linear dynamics of linear  
856 entangled polymers,” *Macromolecules* **35**, 6332–6343 (2002).

857 <sup>39</sup>R. S. Graham, A. E. Likhtman, T. C. B. McLeish, and S. T. Milner, “Microscopic theory  
858 of linear, entangled polymer chains under rapid deformation including chain stretch and  
859 convective constraint release,” *J. Rheol.* **47**, 1171–1200 (2003).

This is the author's peer reviewed, accepted manuscript. However, the online version of record will be different from this version once it has been copyedited and typeset.

PLEASE CITE THIS ARTICLE AS DOI: 10.1122/1.5111111

- 860 <sup>40</sup>M. H. N. Sefiddashti, B. J. Edwards, and B. Khomami, “Individual chain dynamics of a  
861 polyethylene melt undergoing steady shear flow,” *J. Rheol.* **59**, 119 (2015).
- 862 <sup>41</sup>M. Mohagheghi and B. Khomami, “Elucidating the flow-microstructure coupling in the  
863 entangled polymer melts. part i: Single chain dynamics in shear flow,” *J. Rheol.* **60**, 849–  
864 859 (2016).
- 865 <sup>42</sup>M. Mohagheghi and B. Khomami, “Elucidating the flow-microstructure coupling in the  
866 entangled polymer melts. part ii: Molecular mechanism of shear banding,” *J. Rheol.* **60**,  
867 861–872 (2016).
- 868 <sup>43</sup>Q. Huang, J. Ahn, D. Parisi, T. Chang, O. Hassager, S. Panyukov, M. Rubinstein, and  
869 D. Vlassopoulos, “Unexpected stretching of entangled ring macromolecules,” *Phys. Rev.*  
870 *Lett.* **122**, 208001 (2019).
- 871 <sup>44</sup>T. C. O’Connor, T. Ge, M. Rubinstein, and G. S. Grest, “Topological linking drives  
872 anomalous thickening of ring polymers in weak extensional flows,” *Phys. Rev. Lett.* **124**,  
873 027801 (2020).
- 874 <sup>45</sup>A. Bonato, D. Marenduzzo, and D. Michieletto, “Simplifying topological entanglements  
875 by entropic competition of slip-links,” *Phys. Rev. Research* **3**, 043070 (2021).
- 876 <sup>46</sup>P. G. Khalatur and D. A. Mologin, “Rheological properties of self-associating polymer  
877 systems: Nonequilibrium molecular dynamics simulation,” *J. Mol. Liq.* **91**, 205–217 (2001).
- 878 <sup>47</sup>S. Mohottalalage, M. Senanayake, T. O’Connor, G. Grest, and D. Perahia, “Nonlinear  
879 elongation flows effects on aggregation in associating polymer melts,” *Bull. Am. Phys. Soc.*  
880 (2021).
- 881 <sup>48</sup>M. E. Shivokhin, T. Narita, L. Talini, A. Habicht, S. Seiffert, T. Indei, and J. D. Schieber,  
882 “Interplay of entanglement and association effects on the dynamics of semidilute solutions  
883 of multisticker polymer chains,” *J. Rheo.* **61**, 1231–1241 (2017).
- 884 <sup>49</sup>V. A. H. Boudara and D. J. Read, “Stochastic and preaveraged nonlinear rheology models  
885 for entangled telechelic starpolymers,” *J. Rheol.* **61**, 339–362 (2017).
- 886 <sup>50</sup>G. Cui, V. A. H. Boudara, Q. Huang, G. P. Baeza, A. J. Wilson, O. Hassager, D. J.  
887 Read, and J. Mattsson, “Linear shear and nonlinear extensional rheology of unentangled  
888 supramolecular side-chain polymers,” *J. Rheol.* **62**, 1155–1174 (2018).
- 889 <sup>51</sup>C. C. Hua and J. D. Schieber, “Segment connectivity, chain-length breathing, segmen-  
890 tal stretch, and constraint release in reptation models. i. theory and single-step strain  
891 predictions.” *J. Chem. Phys.* **109**, 10018 (1998).

This is the author's peer reviewed, accepted manuscript. However, the online version of record will be different from this version once it has been copyedited and typeset.

PLEASE CITE THIS ARTICLE AS DOI: 10.1122/1.511111

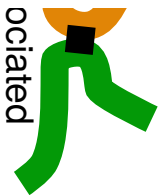
- 892 <sup>52</sup>S. Shanbhag, R. Larson, J.-I. Takimoto, and M. Doi, “Deviations from dynamic dilution  
893 in the terminal relaxation of star polymers.” *Phys. Rev. Lett.* **87**, 195502 (2001).
- 894 <sup>53</sup>M. Doi and J.-I. Takimoto, “Molecular modelling of entanglement.” *Philos. Trans. R. Soc.*  
895 **361**, 641–652 (2003).
- 896 <sup>54</sup>J. D. Schieber, J. Neergaard, and S. Gupta, “A full-chain, temporary network model with  
897 sliplinks, chain-length fluctuations, chain connectivity and chain stretching,” *J. Rheol.* **47**,  
898 213–233 (2003).
- 899 <sup>55</sup>A. E. Likhtman, “Single-chain slip-link model of entangled polymers: Simultaneous de-  
900 scription of neutron spin-echo, rheology, and diffusion,” *Macromolecules* **38**, 6128–6139  
901 (2005).
- 902 <sup>56</sup>M. Andreev and G. C. Rutledge, “A slip-link model for rheology of entangled polymer  
903 melts with crystallization,” *J. Rheol.* **64**, 213–222 (2020).
- 904 <sup>57</sup>J. M. Dealy, D. J. Read, and R. G. Larson, *Structure and Rheology of Molten Polymers*  
905 (Hanser, Munich, 2018).
- 906 <sup>58</sup>M. Doi and S. F. Edwards, *The Theory of Polymer Dynamics* (Clarendon, Oxford, 1986).
- 907 <sup>59</sup>M. Andreev, R. N. Khaliullin, R. J. A. Steenbakkens, and J. D. Schieber, “Approximations  
908 of the discrete slip-link model and their effect on nonlinear rheology predictions,” *J. Rheo.*  
909 **57**, 535–557 (2013).
- 910 <sup>60</sup>A. Cohen, “A padé approximant to the inverse langevin function,” *Rheol. Acta* **30**, 270–273  
911 (1991).
- 912 <sup>61</sup>M. Rubinstein and A. N. Semenov, “Thermoreversible gelation in solutions of associating  
913 polymers. 2. linear dynamics,” *Macromolecules* **31**, 1386–1397 (1998).
- 914 <sup>62</sup>C. Raffaelli, A. Bose, C. H. M. P. Vrusch, S. Ciarella, T. Davris, N. B. Tito, A. V. Lyulin,  
915 W. G. Ellenbroek, and C. Storm, *Rheology, Rupture, Reinforcement and Reversibility:*  
916 *Computational Approaches for Dynamic Network Materials* (Springer, Cham, 2020).
- 917 <sup>63</sup>R. Vinu and L. J. Broadbelt, “Unraveling reaction pathways and specifying reaction ki-  
918 netics for complex systems,” *Annu. Rev. Chem. Biomol. Eng.* **3**, 29–54 (2012).
- 919 <sup>64</sup>J. J. Lukkien, J. P. L. Segers, P. A. J. Hilbers, R. J. Gelten, and A. P. J. Jansen, “Efficient  
920 monte carlo methods for the simulation of catalytic surface reactions,” *Physical Review E*  
921 **58**, 2598–2610 (1998).
- 922 <sup>65</sup>K. Binder and D. Heermann, *Monte Carlo Simulation in Statistical Physics*, 5th ed.  
923 (Springer-Verlag, Berlin Heidelberg, 2019).

This is the author's peer reviewed, accepted manuscript. However, the online version of record will be different from this version once it has been copyedited and typeset.

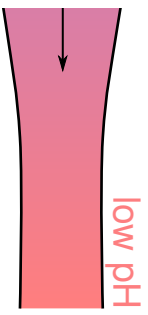
PLEASE CITE THIS ARTICLE AS DOI: 10.1122/1.50000411

- 924 <sup>66</sup>A. P. J. Jansen, *An introduction to kinetic Monte Carlo simulations of surface reactions*,  
925 1st ed. (Springer-Verlag, Berlin Heidelberg, 2012).
- 926 <sup>67</sup>J. Ramírez, S. K. Sukumaran, B. Vorselaars, and A. E. Likhtman, “Efficient on the fly  
927 calculation of time correlation functions in computer simulations,” *J. Chem. Phys.* **133**,  
928 154103 (2010).
- 929 <sup>68</sup>R. M. L. Evans, M. Tassieri, D. Auhl, and T. A. Waigh, “Direct conversion of rheological  
930 compliance measurements into storage and loss moduli,” *Phys. Rev. E* **80**, 012501 (2009).
- 931 <sup>69</sup>T. F. A. de Greef, M. M. J. Smulders, M. Wolffs, A. P. H. J. Schenning, R. P. Sijbesma,  
932 and E. W. Meijer, “Supramolecular polymerization,” *Chem. Rev.* **109**, 5687–5754 (2009).
- 933 <sup>70</sup>A. Koepfel, P. R. Laity, and C. Holland, “The influence of metal ions on native silk  
934 rheology,” *Acta Biomaterialia* **117**, 204 (2020).
- 935 <sup>71</sup>M. Saito and M. Matsumoto, “Simd-oriented fast mersenne twister: a 128-bit pseudoran-  
936 dom number generator,” in *Monte Carlo and Quasi-Monte Carlo Methods 2006*, edited by  
937 A. Keller, S. Heinrich, and H. Niederreiter (Springer Berlin Heidelberg, Berlin, Heidelberg,  
938 2008) pp. 607–622.

sw processing



ociated



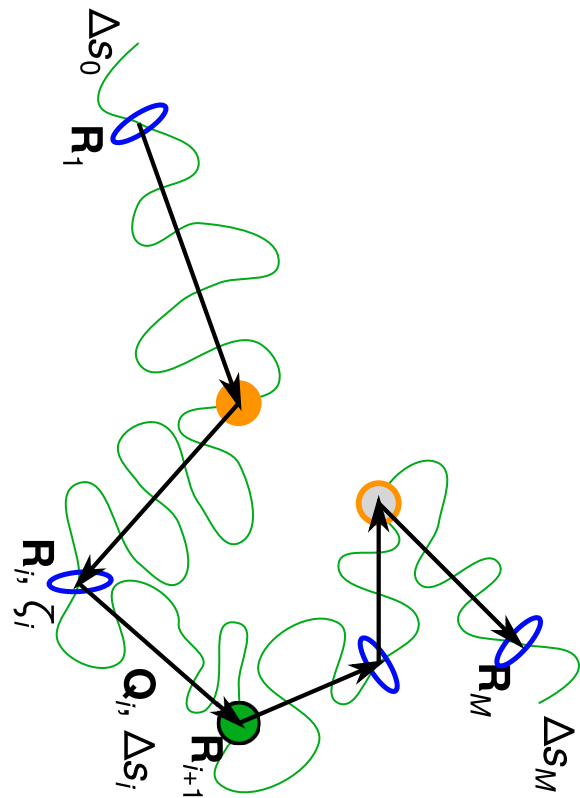
low pH

: associations  
ymental stretching



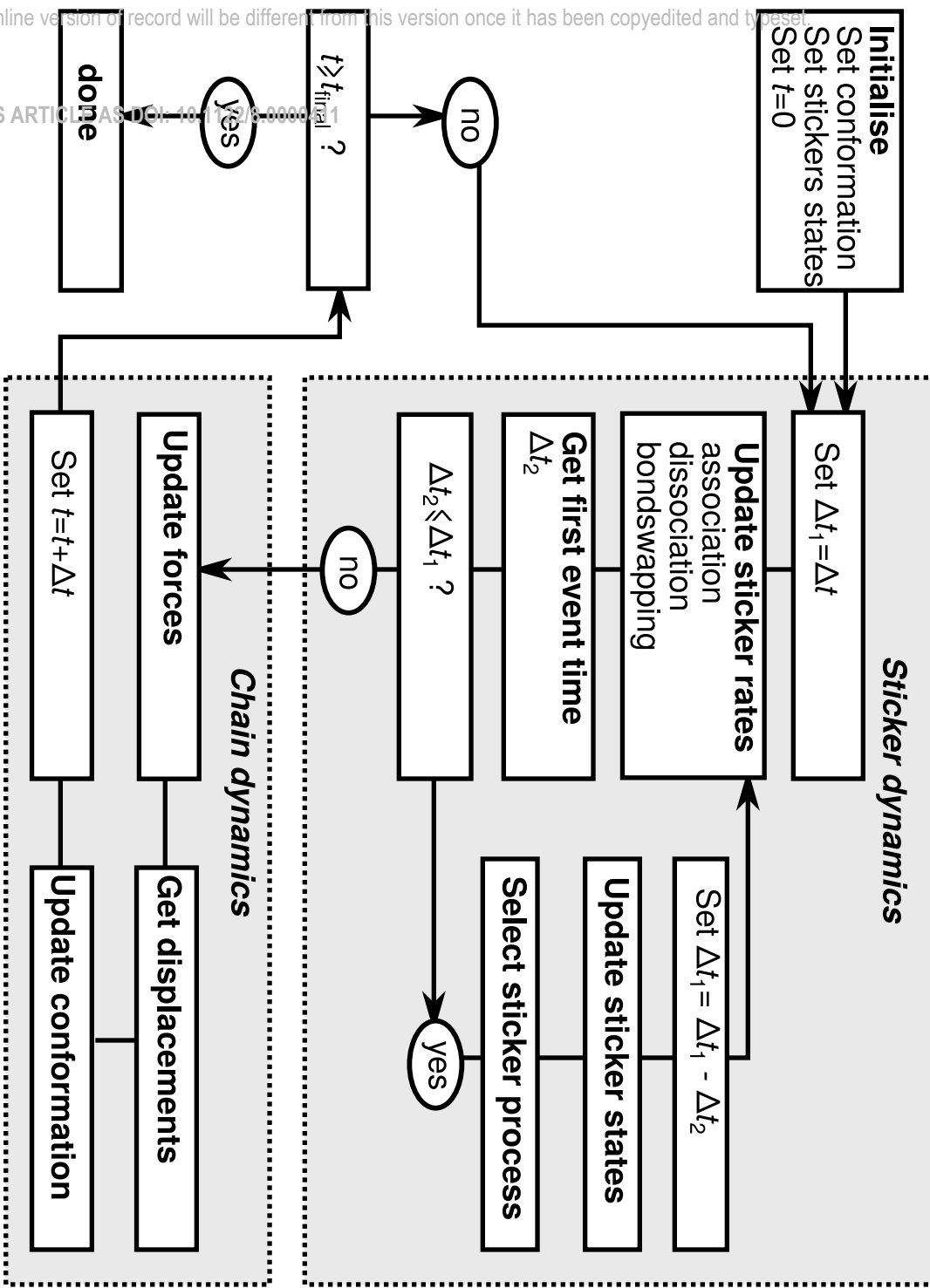
This is the author's peer reviewed, accepted manuscript. However, the online version of record will be different from this version once it has been copyedited and typeset.

PLEASE CITE THIS ARTICLE AS DOI: 10.1122/8.0000411



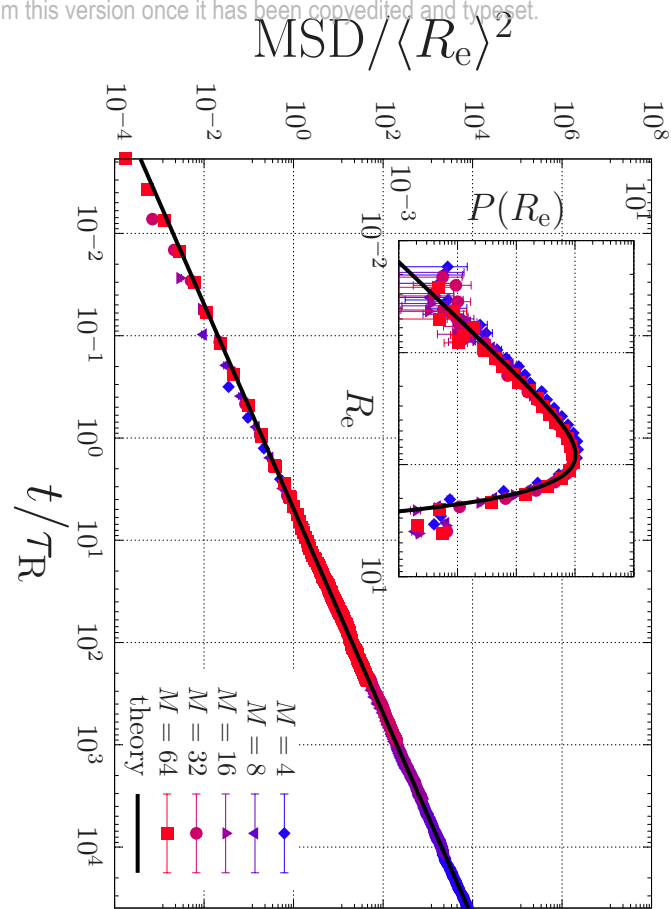
This is the author's peer reviewed, accepted manuscript. However, the online version of record will be different from this version once it has been copyedited and typeset.

PLEASE CITE THIS ARTICLE AS DOI: 10.1177/0898010111411111



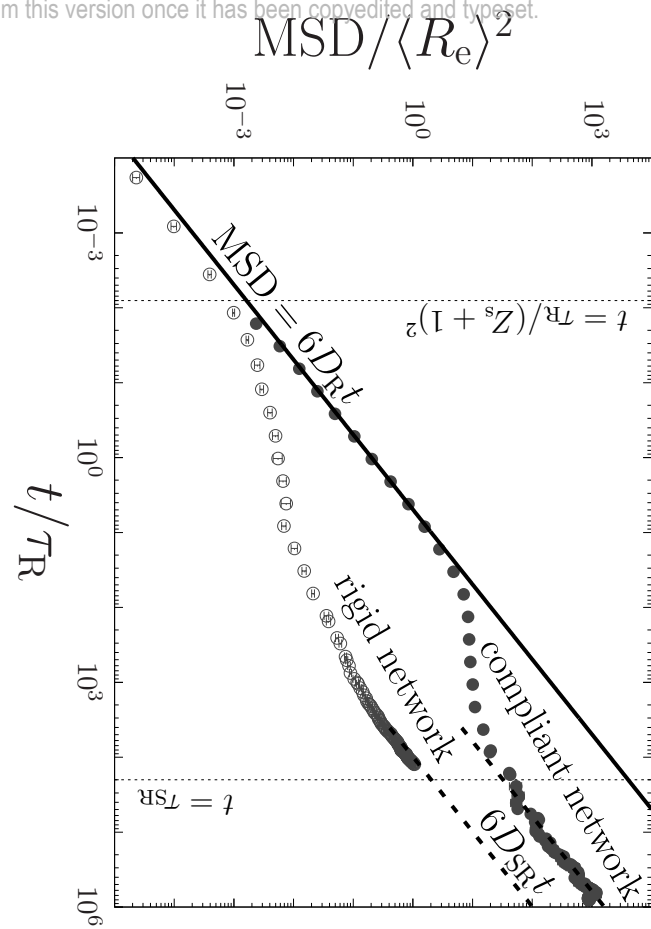
This is the author's peer reviewed, accepted manuscript. However, the online version of record will be different from this version once it has been copyedited and typeset.

PLEASE CITE THIS ARTICLE AS DOI: 10.1122/8.0000411



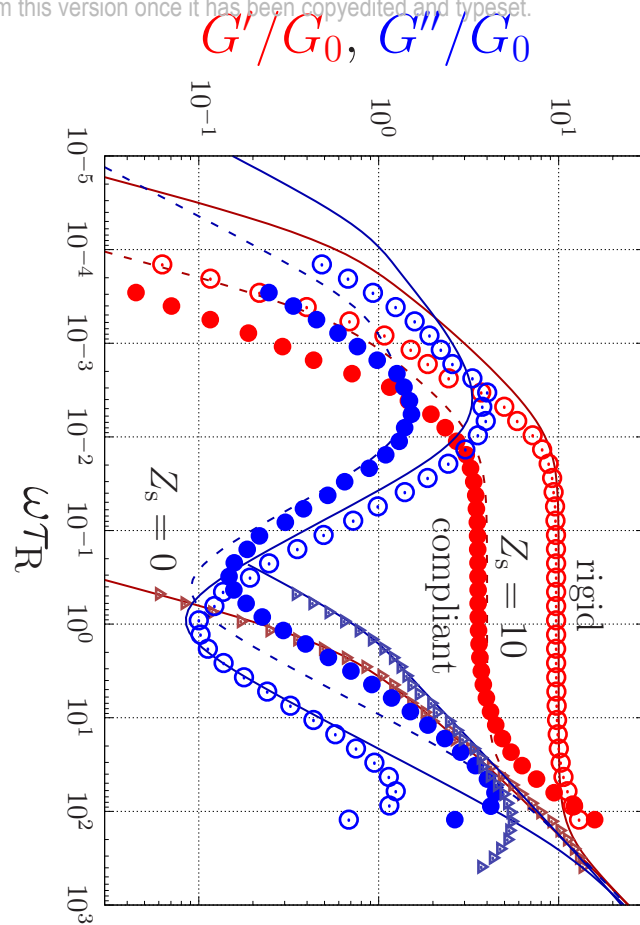
This is the author's peer reviewed, accepted manuscript. However, the online version of record will be different from this version once it has been copyedited and typeset.

PLEASE CITE THIS ARTICLE AS DOI: 10.1122/8.0000411



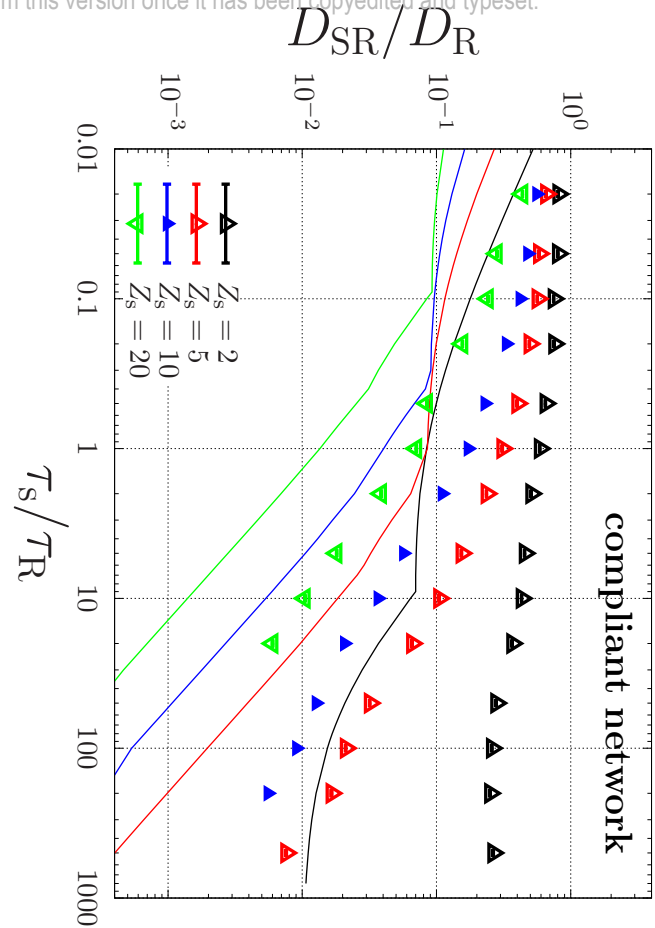
This is the author's peer reviewed, accepted manuscript. However, the online version of record will be different from this version once it has been copyedited and typeset.

PLEASE CITE THIS ARTICLE AS DOI: 10.1122/8.0000411



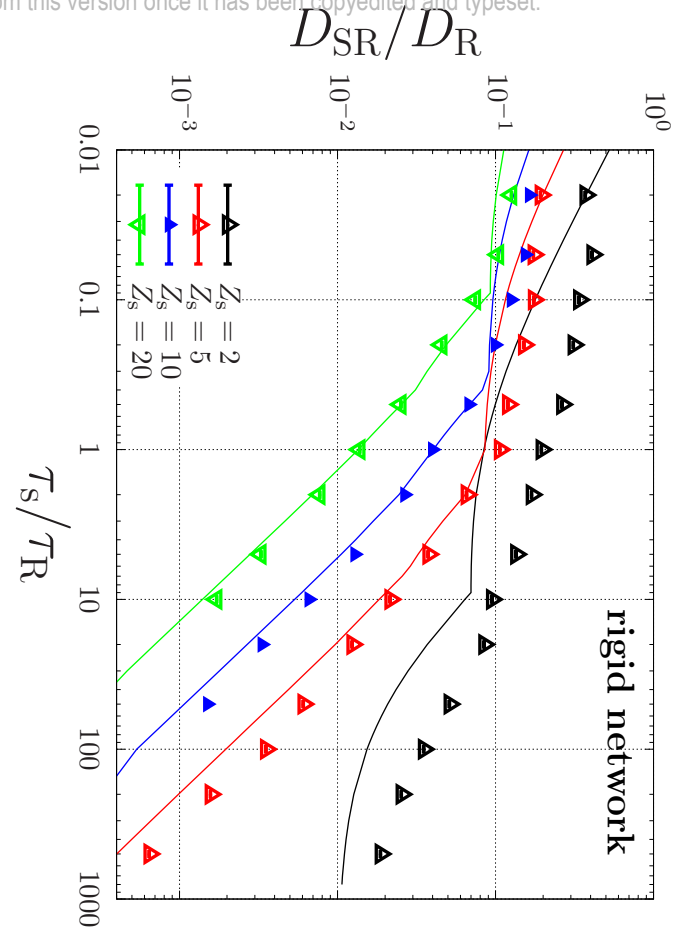
This is the author's peer reviewed, accepted manuscript. However, the online version of record will be different from this version once it has been copyedited and typeset.

PLEASE CITE THIS ARTICLE AS DOI: 10.1122/8.0000411



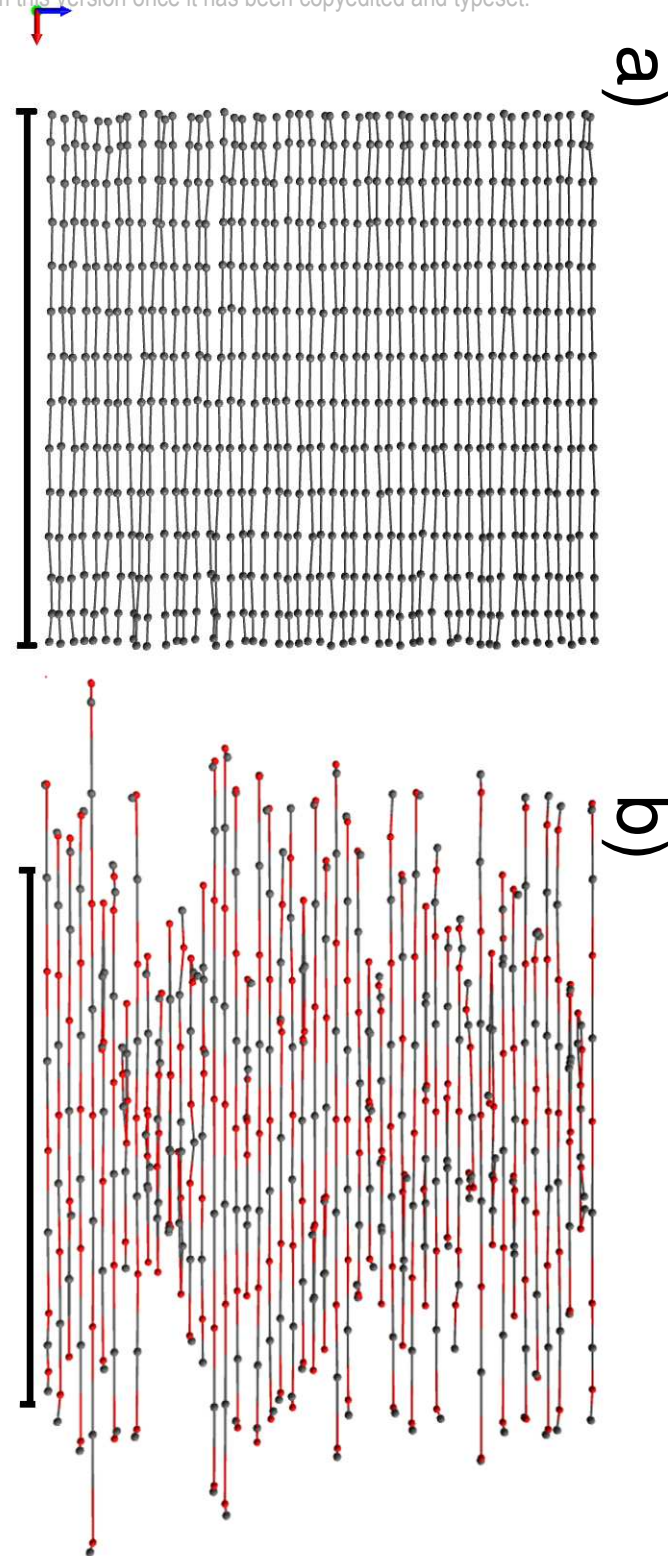
This is the author's peer reviewed, accepted manuscript. However, the online version of record will be different from this version once it has been copyedited and typeset.

PLEASE CITE THIS ARTICLE AS DOI: 10.1122/8.0000411



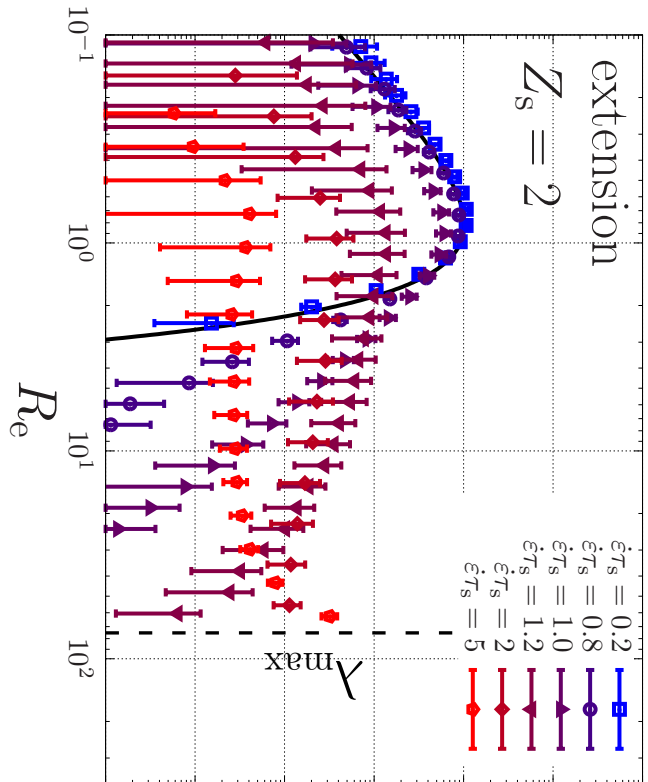
This is the author's peer reviewed, accepted manuscript. However, the online version of record will be different from this version once it has been copyedited and typeset.

PLEASE CITE THIS ARTICLE AS DOI: 10.1122/8.0000411



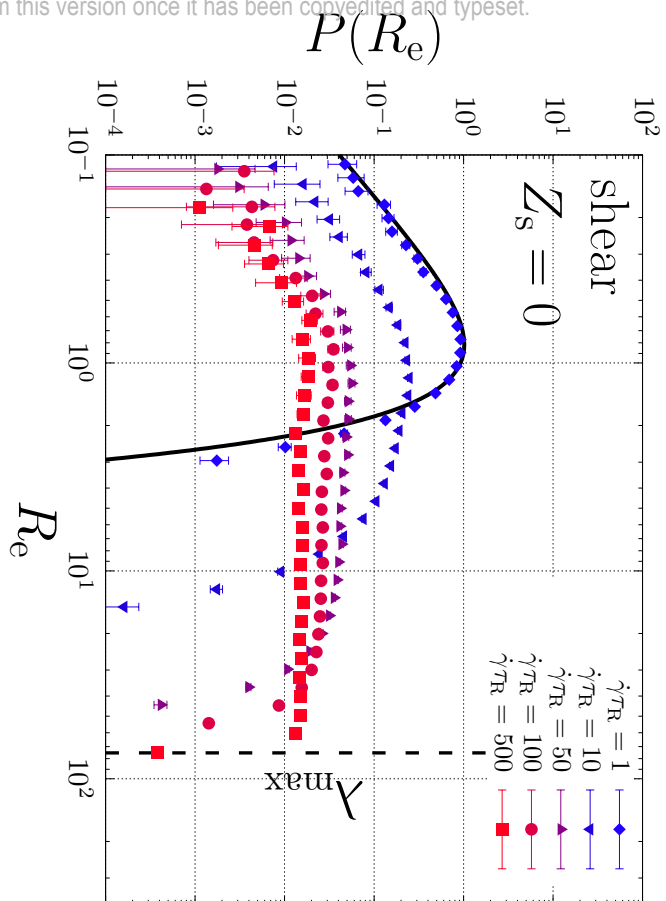
This is the author's peer reviewed, accepted manuscript. However, the online version of record will be different from this version once it has been copyedited and typeset.

PLEASE CITE THIS ARTICLE AS DOI: 10.1122/8.0000411



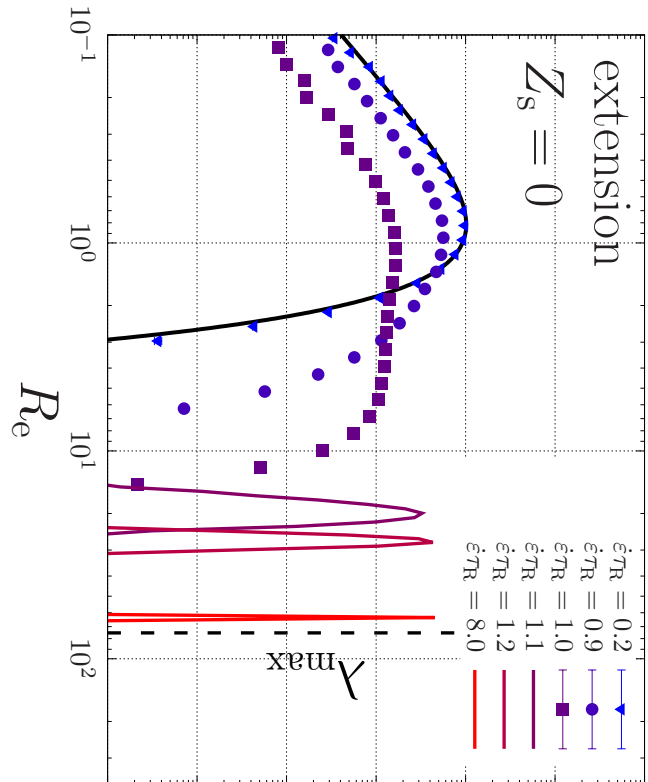
This is the author's peer reviewed, accepted manuscript. However, the online version of record will be different from this version once it has been converted and typeset.

PLEASE CITE THIS ARTICLE AS DOI: 10.1122/8.0000411



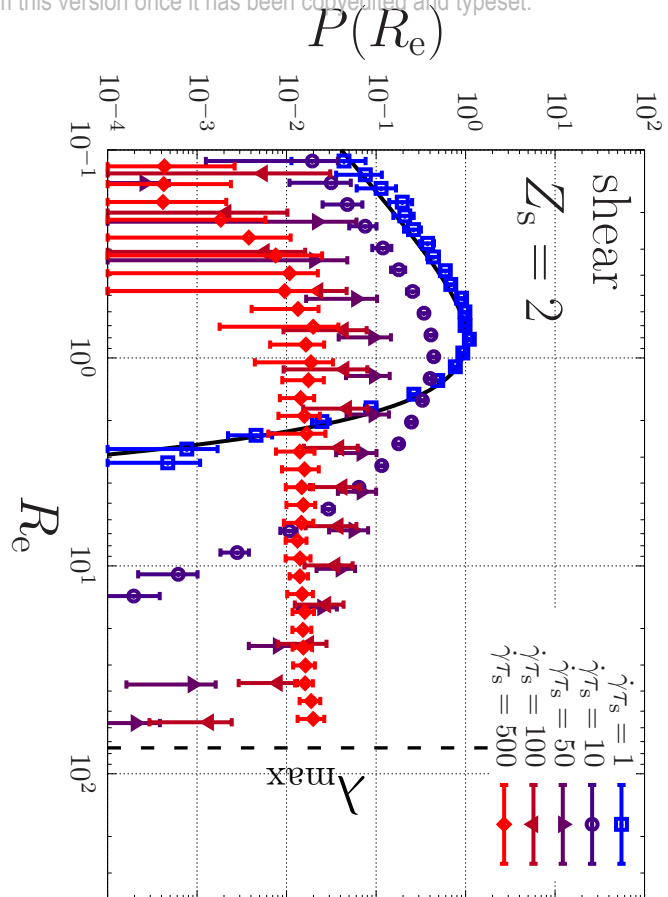
This is the author's peer reviewed, accepted manuscript. However, the online version of record will be different from this version once it has been copyedited and typeset.

PLEASE CITE THIS ARTICLE AS DOI: 10.1122/8.0000411



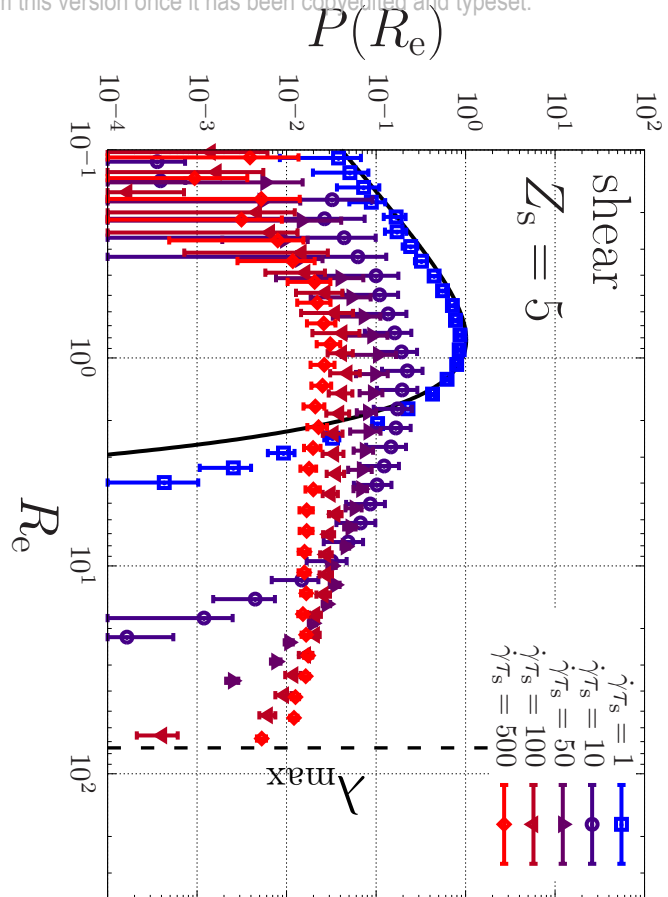
This is the author's peer reviewed, accepted manuscript. However, the online version of record will be different from this version once it has been converted and typeset.

PLEASE CITE THIS ARTICLE AS DOI: 10.1122/8.0000411



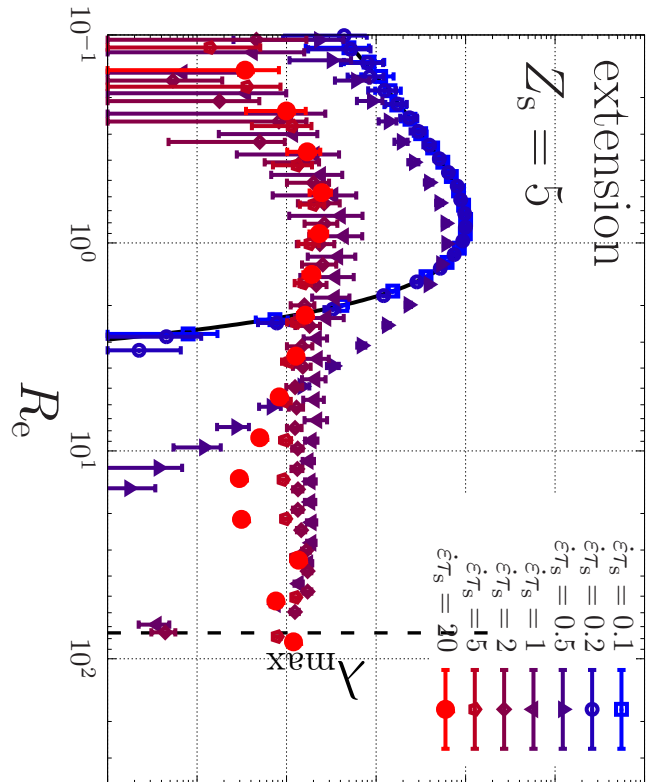
This is the author's peer reviewed, accepted manuscript. However, the online version of record will be different from this version once it has been converted and typeset.

PLEASE CITE THIS ARTICLE AS DOI: 10.1122/8.0000411



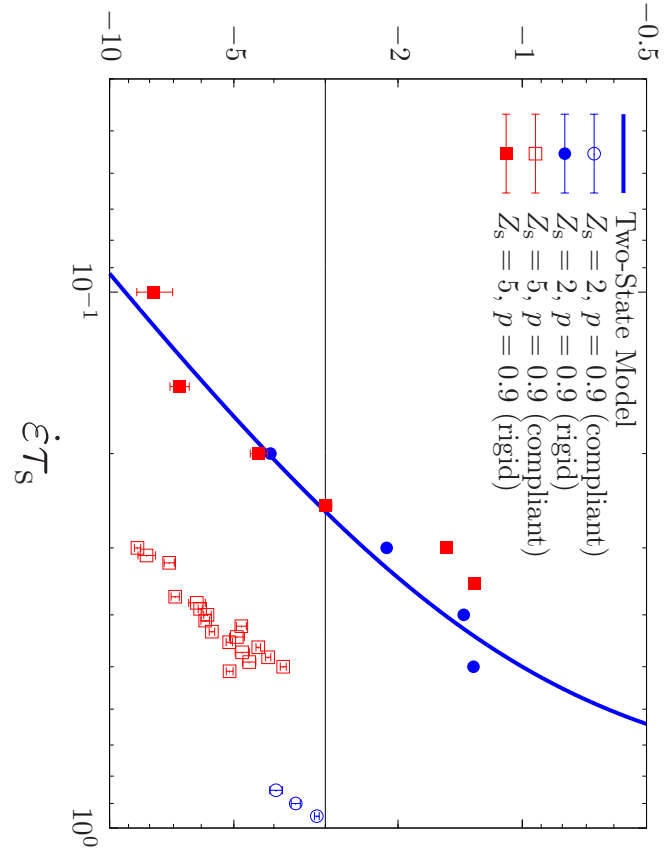
This is the author's peer reviewed, accepted manuscript. However, the online version of record will be different from this version once it has been copyedited and typeset.

PLEASE CITE THIS ARTICLE AS DOI: 10.1122/8.0000411



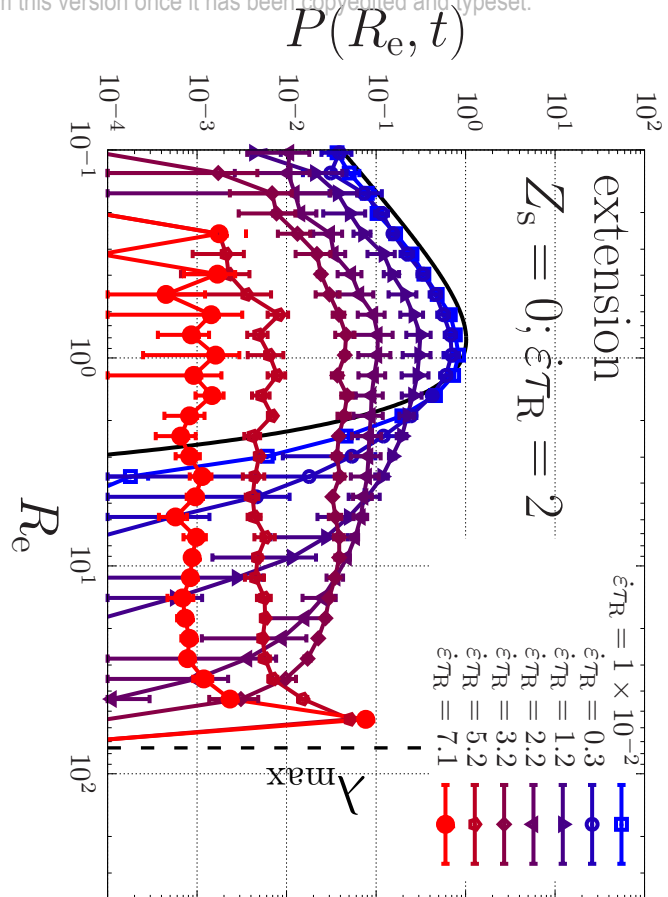
This is the author's peer reviewed, accepted manuscript. However, the online version of record will be different from this version once it has been copyedited and typeset.

PLEASE CITE THIS ARTICLE AS DOI: 10.1122/8.0000411



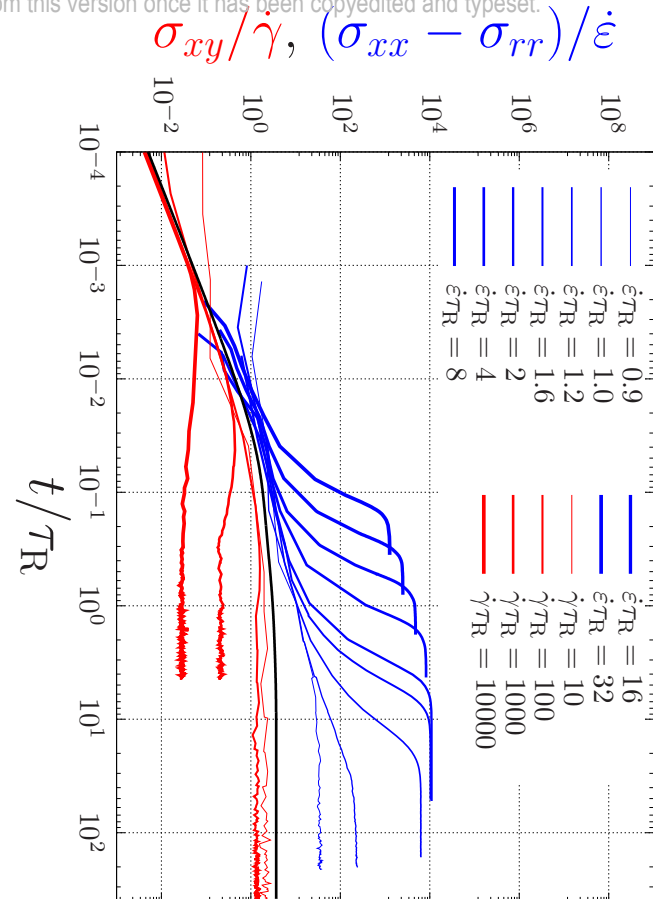
This is the author's peer reviewed, accepted manuscript. However, the online version of record will be different from this version once it has been copyedited and typeset.

PLEASE CITE THIS ARTICLE AS DOI: 10.1122/8.0000411



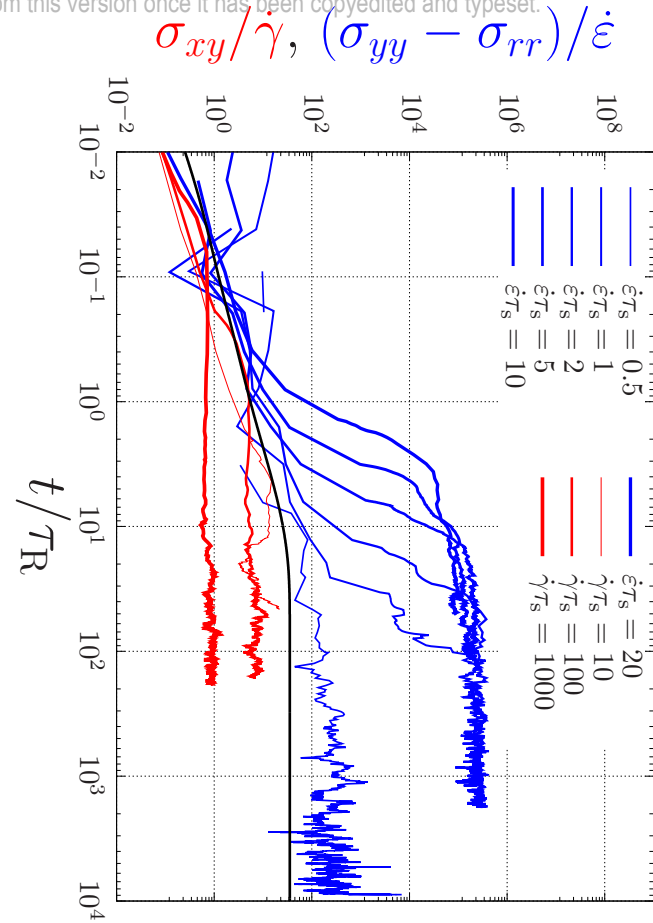
This is the author's peer reviewed, accepted manuscript. However, the online version of record will be different from this version once it has been copyedited and typeset.

PLEASE CITE THIS ARTICLE AS DOI: 10.1122/8.0000411



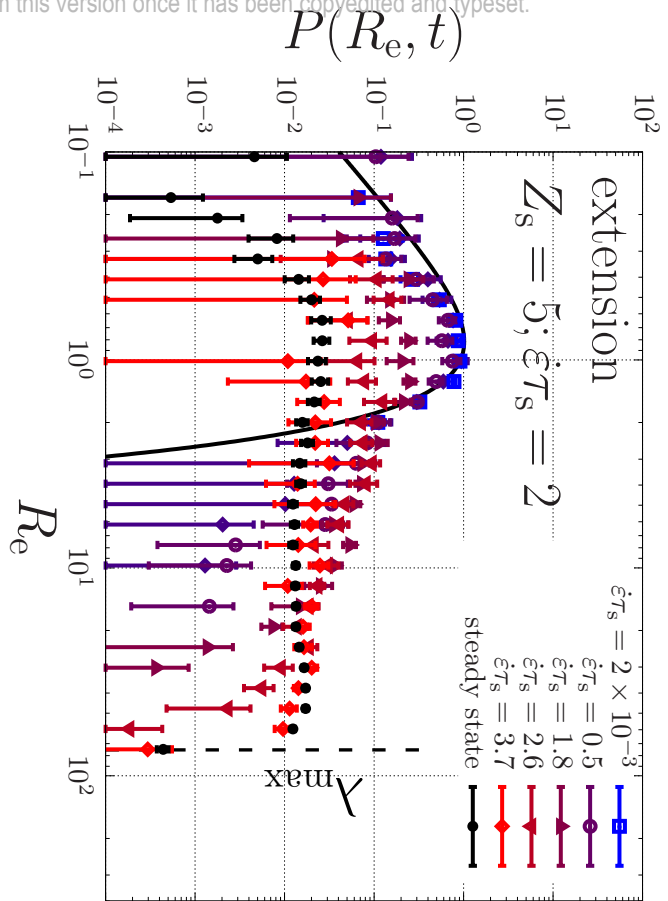
This is the author's peer reviewed, accepted manuscript. However, the online version of record will be different from this version once it has been copyedited and typeset.

PLEASE CITE THIS ARTICLE AS DOI: 10.1122/8.0000411



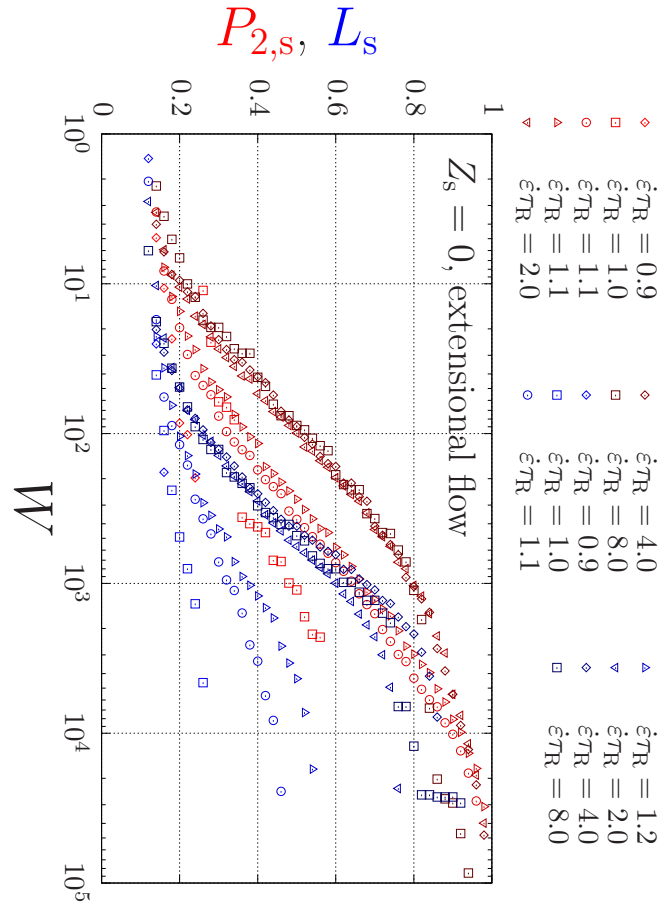
This is the author's peer reviewed, accepted manuscript. However, the online version of record will be different from this version once it has been copyedited and typeset.

PLEASE CITE THIS ARTICLE AS DOI: 10.1122/8.0000411



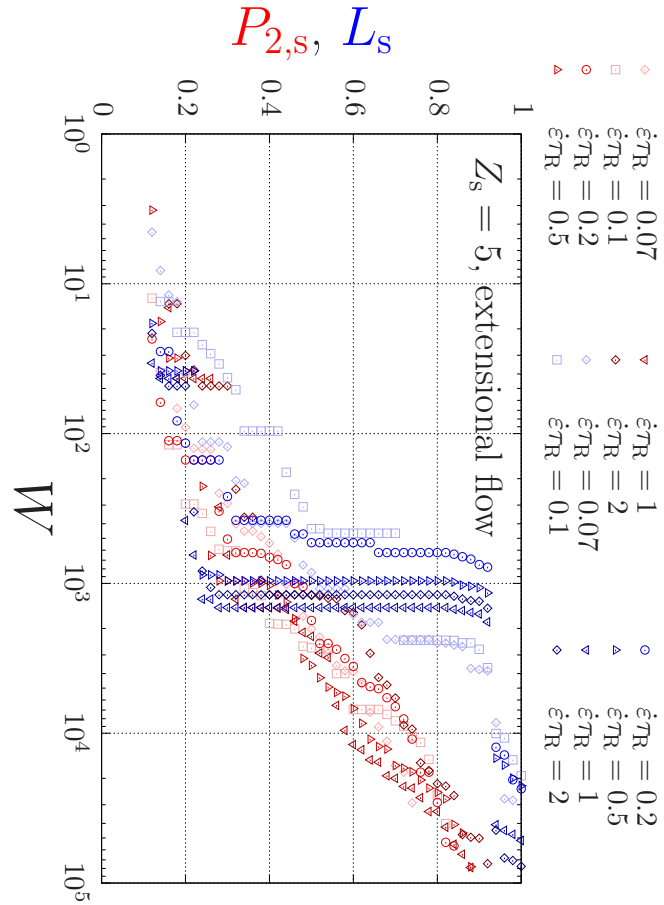
This is the author's peer reviewed, accepted manuscript. However, the online version of record will be different from this version once it has been copyedited and typeset.

PLEASE CITE THIS ARTICLE AS DOI: 10.1122/8.0000411



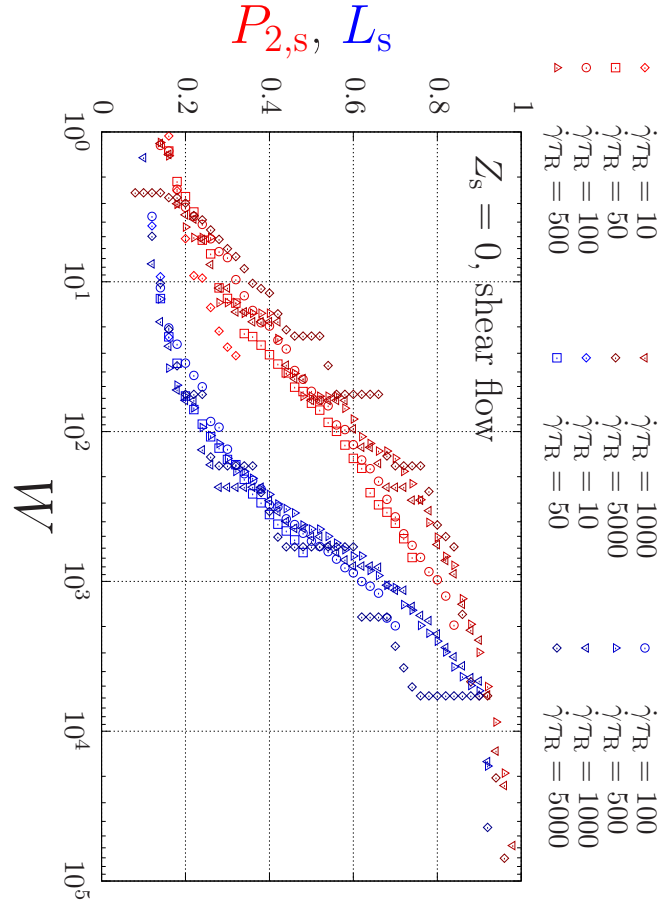
This is the author's peer reviewed, accepted manuscript. However, the online version of record will be different from this version once it has been copyedited and typeset.

PLEASE CITE THIS ARTICLE AS DOI: 10.1122/8.0000411



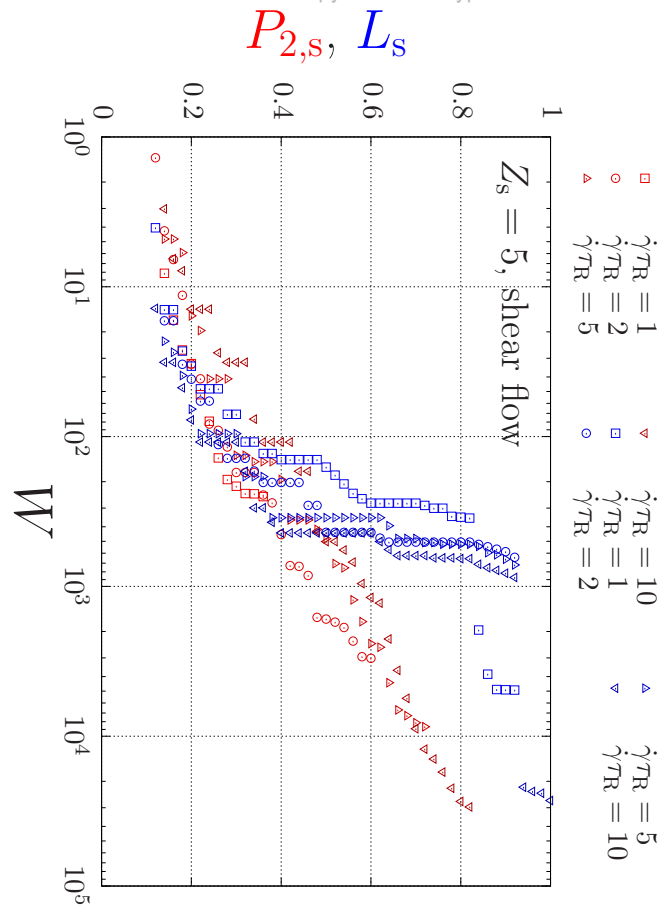
This is the author's peer reviewed, accepted manuscript. However, the online version of record will be different from this version once it has been copyedited and typeset.

PLEASE CITE THIS ARTICLE AS DOI: 10.1122/8.0000411



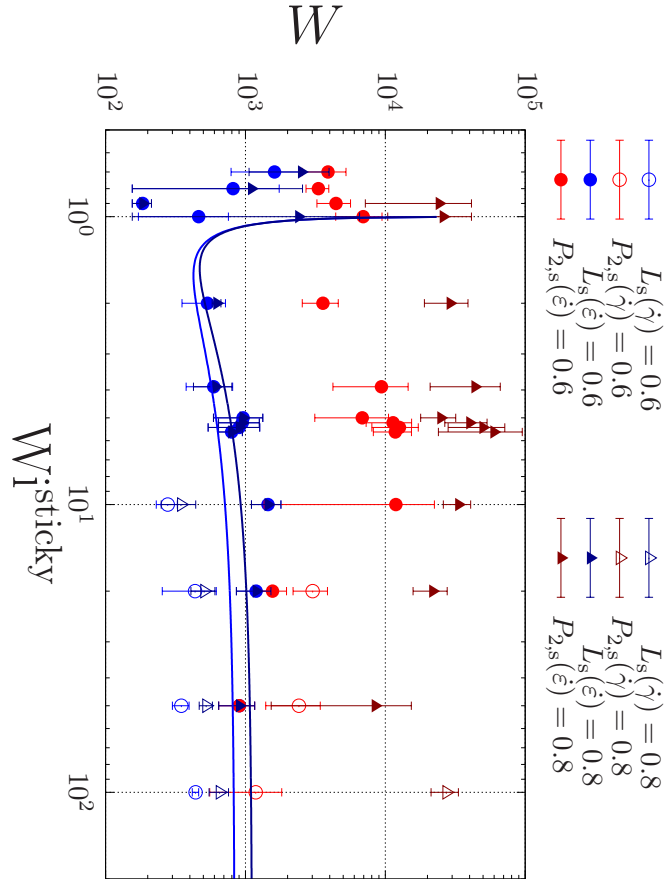
This is the author's peer reviewed, accepted manuscript. However, the online version of record will be different from this version once it has been copyedited and typeset.

PLEASE CITE THIS ARTICLE AS DOI: 10.1122/8.0000411



This is the author's peer reviewed, accepted manuscript. However, the online version of record will be different from this version once it has been copyedited and typeset.

PLEASE CITE THIS ARTICLE AS DOI: 10.1122/8.0000411



This is the author's peer reviewed, accepted manuscript. However, the online version of record will be different from this version once it has been copyedited and typeset.

PLEASE CITE THIS ARTICLE AS DOI: 10.1122/8.0000411

